Research and Development of Low-Profile, Small-Footprint Antennas for VHF-UHF

Range Applications

by

Olusola O. Olaode

Department of Electrical and Computer Engineering
Duke University

Date:_______________________
Approved:

____
William T. Joines, Supervisor

____
W. Devereux Palmer

____
Rhett George

____
Gary Ybarra

____
William M. Reichert

Dissertation submitted in partial fulfillment of
the requirements for the degree of Doctor of Philosophy in the Department of
Electrical and Computer Engineering in the Graduate School
of Duke University

2012

ABSTRACT

Research and Development of Low-Profile, Small-Footprint Antennas for VHF-UHF Range Applications

by

Olusola O. Olaode

Department of Electrical and Computer Engineering
Duke University

Date:________________________
Approved:

____
William T. Joines, Supervisor

____
W. Devereux Palmer

____
Rhett George

____
Gary Ybarra

____
William M. Reichert

An abstract of a dissertation submitted in partial
fulfillment of the requirements for the degree
of Doctor of Philosophy in the Department of
Electrical and Computer Engineering in the Graduate School
of Duke University

2012

Abstract

Research and development of efficient, but low-profile and small-footprint antennas for VHF-UHF range applications remains an ongoing work. VHF range spans 30 – 300 MHz while UHF ranges from 0.3 - 3 GHz. The inverse relationship between the physical length and resonant frequency of an antenna, which is a measure of its operating frequency range, is well known. A direct correlation between an antenna's physical length and radiation efficiency has also been established. Therefore, a combination of these constraints complicates the design of low-frequency antennas that are physically small but with enough radiation resistance to be an efficient radiator. Given the frequency bands above, their corresponding wavelengths will be: 1-10 m (VHF) and 0.1-1 m (UHF). While small-sized antennas in the upper UHF range are relatively easier to prototype, size considerations are necessary with decreasing operating frequency. The length of an antenna operating at these wavelengths would need to be electrically-small, especially at VHF wavelengths given size constraints in applications such as defense or commercial mobile communication. As a consequence, the radiation efficiency of the antenna, which is a function of its radiation resistance, is greatly reduced. In other words, the input impedance or radiation impedance (assuming negligible ohmic losses in the antenna structure) features a small resistive component and a large capacitive component, causing reflections of most of the incident power to

the antenna. Highly-reactive antennas are not desired for most transmitters and receivers. Therefore, the radiation resistance of an antenna must be increased by increasing its electrical length while simultaneously maintaining a low profile and footprint. This aim can be achieved by configuring the antenna to excite a resonance at, or very close to a desired operating frequency. An approach that I will explore in this dissertation is to exploit the broadband characteristics of meander-line and helical (or "spiral") antennas typically applied in the upper UHF-microwave frequency range to the lower frequencies. I will also propose novel antenna geometries that combine spiral and meander-line properties and analyze their performance via their return losses. Return loss is a reliable measure of the impedance match by an antenna to its preceding circuitry at different frequencies or, a ratio of the reflected power at the antenna load to the incident power. These antennas offer significant size reductions; for example, a bowtie meander dipole antenna studied yielded a height reduction of 55% at 64 MHz relative to a half-wave dipole antenna of the same resonant frequency. In addition, I will present a set of equations developed for predicting the fundamental resonant frequency and radiation resistance of meander-line antennas.

The body of work presented here has been featured in several peer-reviewed publications. They are included here for convenient reference:

- O. O. Olaode, W. D. Palmer, and W. T. Joines, "Evaluating the Efficiency of the Digitally-Driven Antenna Architecture," *IEEE International Symposium on Antennas* *and Propagation and Union of Radio Science International Meeting*, Charleston, SC – June 2009.

- O. O. Olaode, W. D. Palmer, and W. T. Joines, "Analysis of the Efficiency Improvements of a Directly-Driven Antenna-Based AM Transmitter," *Proceedings of the 2009 Antenna Applications Symposium*, vol. 33, pp. 418-429, Sept. 2009.
- O. O. Olaode, W. D. Palmer, and W. T. Joines, "Improvements of a Directly-Driven Antenna-Based AM Transmitter over the AM Frequency Band," *Proceedings of the 2010 Antenna Applications Symposium*, vol. 34, pp. 372-388, Sept. 2010.
- O. O. Olaode, W. D. Palmer, and W. T. Joines, "Efficiency Improvements of a Directly-Driven Antenna-Based AM Transmitter over the AM Frequency Band," *IEEE Antennas and Propagation Society Meeting*, Spokane, WA, July 2011.
- O. O. Olaode, W. D. Palmer, and W. T. Joines, "Effects of Meandering on Dipole Antenna Resonant Frequency," *IEEE Antennas and Wireless Propagation Letters*, accepted for publication, January 2012.
- O. O. Olaode, W. D. Palmer, and W. T. Joines, "Characterization of Meander Dipole Antennas with Geometry-based, Frequency-independent Lumped Element Model," *IEEE Antennas and Wireless Propagation Letters*, March 2012.
- W. D. Palmer, O. O. Olaode, R. J. Spiegel, and W. T. Joines, "Directly-Driven Antennas from a Circuit Analysis Viewpoint," *Proceedings of the 2011 Antenna Applications Symposium*, September 2011.

Contents

List of Tables

List of Figures

Acknowledgements

I am profoundly grateful to my advisor, Prof. William Joines and my principal investigator, Dr. Devereux Palmer for their unwavering support rendered to me throughout my graduate studies, even during the difficult times. Their personal sacrifices and dedication to my academic success as well as professional development are duly recognized and appreciated. During the last four years, my technical knowledge and understanding of the principles of electromagnetics, especially antennas had been greatly enhanced. Much can still be said about them but above all, I extend my deepest gratitude to them.

I had the privilege of collaborating with Dr. Ronald Spiegel of the department of electrical and computer engineering at Duke on some technical papers and research on Directly-Driven Antennas. It was a truly rewarding experience. His understanding and practical experience of electromagnetics especially fractal antennas has been a valuable resource to me. I thank him for his support.

I also wish to thank the following faculty members who had served in my PhD qualifying exam, PhD preliminary exam, and dissertation defense committees during my studies at Duke for answering the call to serve and for their guidance. They are: Prof. Gary Ybarra (ECE), Prof. Rhett George (Emeritus, ECE), Prof. Monty Reichert (BME), Prof. Fred Boadu (CEE), and Prof. Qing Liu (ECE). ECE is an acronym for *Electrical and Computer Engineering* while CEE is an acronym for *Civil and Environmental Engineering*.

I am grateful to my family for their support and encouragement throughout my studies at Duke, which had been a major source of motivation and strength.

Finally, I wish to thank my lovely wife, Aboyewa Olaode for her support, understanding, dedication, and personal sacrifices towards ensuring the eventual completion of my doctoral studies. She has been an oasis and a source of stability in turbulent times. I am indeed fortunate to be married to you. Many thanks!

1. Introduction

Modern wireless systems increasingly require more compact, portable, wide-band, and efficient transmitter architectures. Designing an antenna to meet these standards at low frequencies is especially difficult to do. Published literature shows that a half-wave dipole antenna, for example, presents a resistance identical to a 75 Ω source (such as a TV antenna) and can be easily matched to a 50 Ω source. In addition, the half-wave dipole impedance possesses a negligible reactive component at a total electrical length of ~0.48-0.49 λ [1]. Thus, the antenna radiates quite effectively at frequencies where the length is near a half wavelength. However, a half wavelength antenna operating at many of the frequencies in the VHF-UHF spectrum would be several meters long. Reducing the size of the antenna while operating at low frequencies will benefit defense and commercial applications alike. However, as a consequence of the size reduction, the antenna's radiation efficiency is adversely impacted [2].

Antenna design engineers have proposed different solutions to the fundamental frequency-physical size conundrum, usually alternative geometries that would increase the electrical length of the antenna but compact the entire structure into its smallest possible volume. Examples of such approaches were Meandering and inverted-F Configurations [3] for line antennas, inductive and capacitive loading for slot antennas [4], [5]. These techniques had been shown to offer bandwidth improvements in the planar, microstrip antenna structures where they had been applied.

However, antenna size reduction effort had mainly been limited to the UHF frequency bands and higher. Therefore, a solution that would be broadband, yet low in profile and easily fabricated in the frequency band below UHF requires further investigation. Such a solution would be of interest to the defense community since a substantial amount of the Army's mobile ground communications are in the VHF-UHF range.

A useful tool in the investigation of enhanced bandwidth, electrically-small antennas is quantitative analysis i.e. employing equations and/or accurate representative models in the design process of an antenna. The antenna configurations considered for the low frequency applications of interest are: conventional meander-line, bowtie meander-line, and spiral. These antennas had been analyzed numerically and experimentally and will be presented later in the dissertation.

In a system that utilizes an antenna, e.g. a transmitter, the bandwidth and efficiency are two of the most important measures of performance. While the antenna is obviously important, it is only a part of a system comprising of other components. Therefore, holistic enhancements to the system should involve improvements to both the antenna and the driver circuitry. That is, the overall efficiency of a system e.g. a transmitter is a function of the antenna efficiency as well as the efficiency of the driver circuit. Alternative transmitter architecture named Directly Driven Antenna, or DDA, was proposed, designed, and analyzed relative to a conventional transmitter at AM frequencies. More on this work in the next chapter. However, it was difficult to evaluate the true performance of the proposed alternative architecture with an electrically-small transmit antenna. Therefore, given the impact of antenna efficiency on the transmitter system, subsequent effort was focused on improving antennas for transmitters operating in the frequency range of US Army ground mobile communication equipment.

2. Directly-Driven Antenna (DDA) Architecture at AM Frequencies

2.1 Overview of the Directly-Driven Antenna (DDA) Architecture

Joseph T. Merenda (Patent # 5,402,133) proposed a system in which a radio signal can be digitized through a pulse width modulator and used to control the switching rate of a pair of complementary transistors in a class D amplifier configuration. The signal is subsequently radiated by electrically small antenna systems (antennas whose physical sizes are small relative to excitation wavelength [6]). This approach was proven to result in improved bandwidth and efficiency in getting signals to the antenna and forms the basis of the work described in this dissertation.

Fig. 1 shows the architecture of the DDA system and its contrast to a conventional AM circuit block diagram. Modulation of an information signal is performed in an identical manner by both the DDA and the conventional systems except that the power amplifier and low-pass filter/matching network stages in the conventional architecture are replaced with a pulse-width modulator and complementary switching transistors in the DDA architecture.

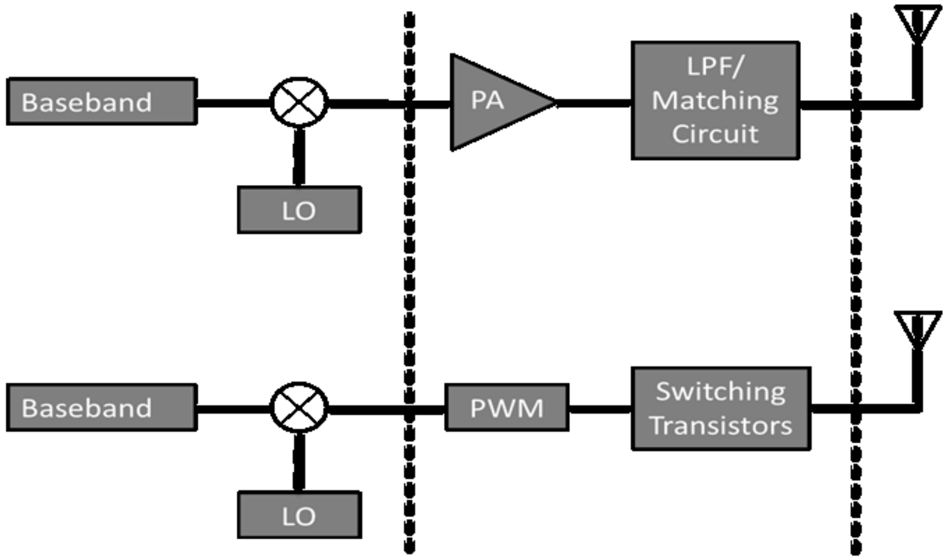

Figure 1: Block diagram showing the architectures of the conventional (upper) and directly-driven antenna (DDA) (lower) AM transmitters. Both circuits transmit a carrier signal (LO) modulated by a baseband signal. The conventional architecture uses a linear power amplifier (PA) and low-pass filter or matching circuit to power to the antenna. The DDA architecture uses a pulse-width modulator and switching transistors to directly drive the antenna with a pulse-width modulated square wave containing the modulated carrier information. Glossary of terms - LO: Local Oscillator, PA: Power Amplifier, PWM: Pulse-Width Modulator, LPF: Low-Pass Filter.

The Pulse Width Modulation (PWM) in the DDA architecture is performed by a comparator amplifier as shown in Fig. 2. A high-frequency local oscillator that has been modulated with a baseband signal (Modulated Carrier, V_{MC}) is driven into the positive terminal of the comparator and sampled through a much-higher frequency sawtooth waveform (Reference, V_{REF}). The output of the comparator is low when the magnitude of the reference exceeds the baseband and high otherwise; hence resulting in the pulse-width modulation. For a given input level, the sawtooth frequency determines the frequency of the comparator's output [7] while the baseband frequency determines its duty cycle. Therefore, for an accurate signal reconstruction, the frequency of the reference waveform should be at least ten times that of the baseband [7].

The digitized version of the modulated carrier signal from the PWM stage discussed in the previous section is driven directly into a pair of complementary bipolar junction transistors driven either in cutoff or saturation shown in Fig. 3. Therefore, the output is a copy of the input pulse train but at a higher current level, oscillating between the amplifier's rail voltages ($+V_S$ and $-V_S$). Furthermore, current spikes are generated only during the transition times of the voltage signal. The information contained in the modulated carrier signal and encoded in the separation of the current spikes is converted to analog by the antenna reactance, radiated and recovered at the receiver end. Because current flows to the antenna only in very short bursts, the power transfer from the transmitter output stage may be increased. Next, I will discuss the application of the proposed (DDA) transmitter design in the AM frequency band.

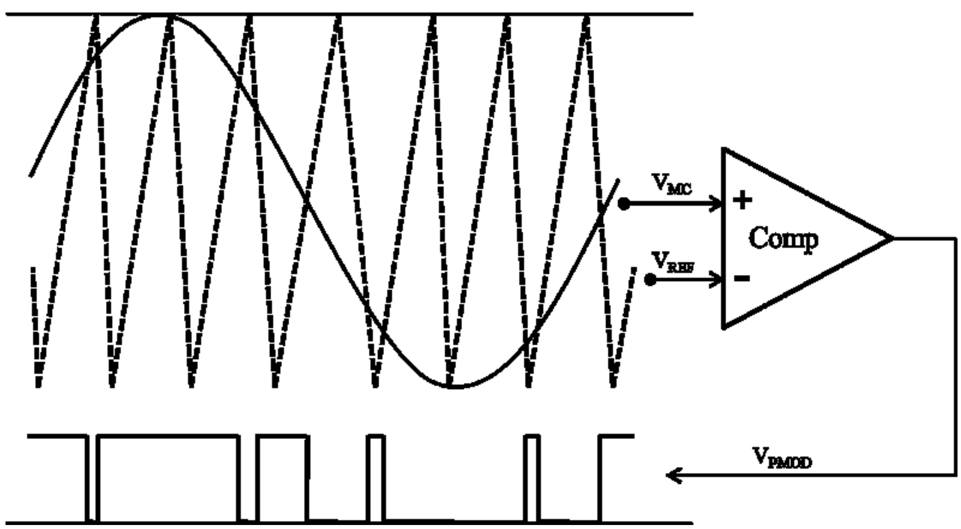

Figure 2: Pulse Width Modulation stage of a Class D Amplifier. A modulated carrier signal (V_{MC}) is sampled with a sawtooth signal (V_{REF}) with 10 times the frequency of MC to produce the square wave signal (V_{PMOD}). Glossary of terms - Comp: Comparator.

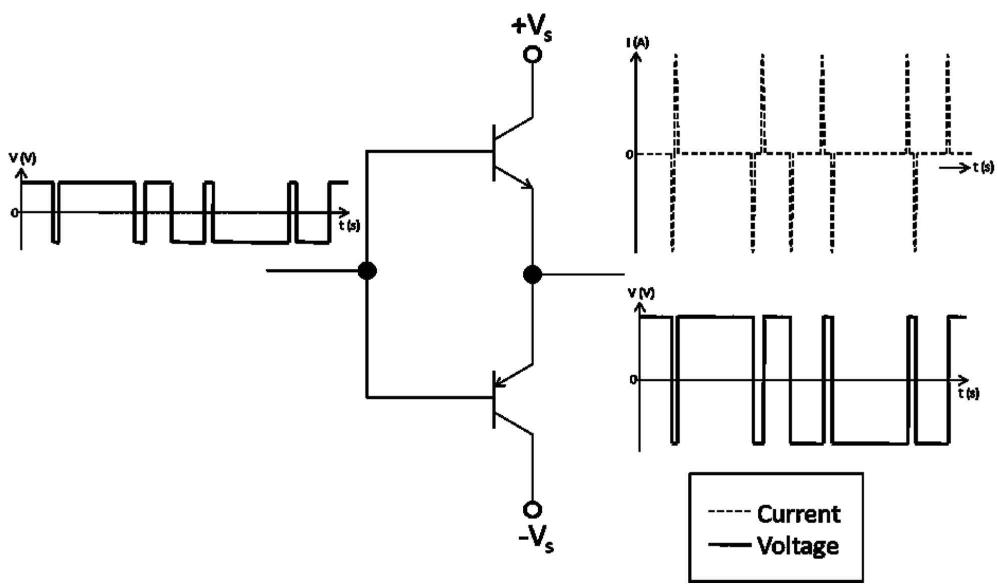

Figure 3: Switching amplifier stage of a Class D amplifier. The VPMOD signal from Fig. 2 is driven into a pair of bipolar switching transistors resulting in the amplification of the signal. When the switching amplifier stage is loaded with an electrically-small antenna, the current waveform shown is generated.

2.2 Performance Improvements of the Directly-Driven Antenna over the Conventional Architecture

In this section, the DDA concept is applied in an AM transmitter and its performance compared to a reference transmitter design called the conventional AM transmitter. Conventional radio transmitters have some well-known limitations: they require an impedance matching network tuned to the carrier frequency and are band limited. Merenda [6] proposed a system to mitigate the limitations presented in *Section 2.1*. Through the use of a highly efficient Class-D amplifier and the regulation of power delivery to a load e.g. antenna, his approach was theoretically shown (but not practically implemented) to result in improved bandwidth and efficiency in terms of getting signals to the antenna. Merenda's approach was then tested in an actual transmitter as described below: A baseband audio signal was modulated with sine waves at each of the following frequencies: 570 kHz, 950 kHz and 1440 kHz. The resulting modulated signal was then sampled (digitized) by a pulse-width modulating (PWM) operational amplifier. The reference frequency of the pulse-width modulator was selected to be ten times the carrier frequency of the local oscillator (see Fig. 1). The Nyquist sampling theorem stipulates the lower bound of the sampling frequency is twice the highest frequency present in the signal to be sampled to facilitate its reconstruction. The square wave output of the PWM stage was then amplified by a Class-D amplifier as indicated in Fig. 2. Class-D amplifiers have been known to achieve efficiencies ranging from 70% to 100% (theoretical value) depending on the power level and the magnitude of switching losses [8]. The switching transistors in the Class-D amplifier generate current spikes that radiate the modulated signal at intervals determined by the duty cycle of its sampled form. An electrically-small dipole antenna (λ/3300 at 1 MHz) was used to radiate the resulting signal. At the frequencies of interest in the AM band, the impedance of the transmit antenna is predominately capacitive. Therefore, it charges and discharges based on the direction of the current spikes that excite the antenna.

To contrast the performance of the DDA design with conventional AM transmitter, it is appropriate for the design of the transmitter to be as identical and realistic as possible to the proposed DDA design. Therefore, the LM386 low-power audio amplifier was used along with low-pass filters tuned to 570 kHz, 950 kHz and 1430 kHz.

2.2.1 Observations

To qualitatively compare the performance of the two AM transmitter architectures, the modulated carrier signals were set to a given power level and the signals received on the portable tabletop AM radio receiver was tuned to each of the three carrier frequencies used for this study. The AM radio was gradually moved away from the dipole (transmit) antenna along the plane of the peak broadside radiation pattern. It is noteworthy to mention that both transmitters reproduced the signal from the music player in a clear, recognizable way although the DDA-based transmitter yielded a much higher-fidelity reproduction of the original signal despite the fact that the DDA architecture does not include an explicit filtering mechanism on the output stage. In addition, the broadcast signal still could be heard a few feet beyond where the signal produced by the conventional transmitter architecture became unintelligible. Given that the testing conditions for the two architectures were otherwise identical, the observation described above signifies that more of the modulated carrier signal power is radiated in the DDA case than in the conventional circuit case. Therefore, these qualitative assessments offer strong evidence that the DDA transmitter produces a more efficient coupling of the signal to the electrically-small transmit antenna.

To further quantify the relative performance, the radiated frequency spectrum was measured at the receive antenna end placed at a distance of 9 cm for each architecture. This distance was chosen such that mutual coupling between transmit and receive antennas is minimal i.e. ensures far field transmission as estimated by (1) [9],

$$R \geq \frac{2d^2}{\lambda} \tag{1}$$

where *R* is the radial distance between transmit and receive antennas and d is the longest linear dimension of the dipole. Also, interference from the test equipment and active transmission lines is minimized through a careful setup of the laboratory. Under identical testing conditions outlined earlier, the power magnitudes in the received waveforms were measured at the following carrier frequencies: 570 kHz, 950 kHz, and ~1430 kHz, for both architectures (DDA and conventional AM transmitters). The results are summarized in Table 1. In each case, care was taken to ensure that the same amount of power, 1.2 mW was delivered from the power supplies to the dipole transmit antenna. Therefore, the received power gains recorded for the DDA case were a function of the electronics in its architecture. As a result, the received power at 1440 kHz was recorded, instead of 1430 kHz. In the case of the DDA transmitter, for each carrier signal frequency, the sawtooth wave frequency is always ten times the selected carrier frequency.

Table 1: Received Power Results

Carrier Frequency (kHz)	Transmit Architecture			
	Conventional AM		DDA	
	(dBm)	(pW)	(dBm)	(pW)
570	-89.33	1.17	-88.44	1.43
950	-91.87	0.65	-82.01	6.30
1430 (conv. AM)/ 1440 (DDA)	-90.74	0.84	-87.56	1.75

According to Table 1, the DDA architecture showed minimal gains at 570 kHz and 1430/1440 kHz, but a much higher gain (9.6X) at 950 kHz. Therefore, it can be concluded that the gain improvement realizable by the DDA technique is carrier-frequency dependent and is largest around 1 MHz. In addition, the results suggested that the DDA architecture produces more efficient coupling of the modulated carrier to an electrically-small transmit antenna. In cases where minimal improvements were recorded, the DDA is still the more versatile transmitter approach in that, the fundamental requirement for a matching circuit is bypassed. Many research questions remain, including analysis and control of the spectral content of the radiated signal, comparison of the relative efficiency, size, and cost of the DDA and conventional architectures, PWM clock rate and stability requirements as a function of modulation complexity, and the effect of the transmit antenna design on the filtering properties of the DDA architecture. The DDA architecture also introduces more fundamental questions, potentially requiring new definitions for standard antenna terms such as "match" and "near field" in the DDA context where the assumptions used in analysis of steady state operation no longer apply. The focus of my study now shifts to investigating the different electrically small antennas configurations that could be used in conjunction with the DDA architecture to improve its performance.

3. Antennas for the DDA

While the DDA transmit architecture has been shown to yield a 9.6X higher radiated power [10] over the conventional architecture, this observation was made with a dipole transmit antenna that is $\lambda/3300$ long with a radiation efficiency of 2.8 % (see Appendix B for the relevant calculations). Therefore, given that the antenna could be electrically longer, more efficient, yet practically applicable, alternative antenna configurations were considered.

3.1 Dipole Antennas: Half-wave and Electrically-small

An antenna is any wire that conducts current. Depending on the specifications, the following parameters are used to characterize or design an antenna: gain, return loss, radiation resistance, bandwidth, etc. Depending on the frequency of operation, antennas vary in geometrical size. One of the most basic antennas is the dipole, which is simple to construct but has the disadvantage of a narrow bandwidth. For a maximum power transfer to an antenna load, the load must be impedance-matched to the stage/device preceding it i.e. the resistive components of the respective impedances must be equal and the reactive components of the impedances must be conjugate of each other. The half-wave dipole is one of the most commonly-used line antennas. As shown in Figure 4, it is center-fed and has an electrical length of $\lambda/4$ on each arm. The input impedance of a half-wave dipole i.e. total length of 0.5 λ is 73 + j42.5 Ω [1]. However, this dipole does in fact resonate at a slightly-lower total length of ~0.49 λ. At this electrical length, the input impedance is 70 +j0 Ω [11]. Assuming that ohmic losses are negligible, the input resistance of an antenna is a first-order approximation of its radiation resistance. Note that the resonant length of an antenna is defined as the electrical length at which the input impedance is purely resistive.

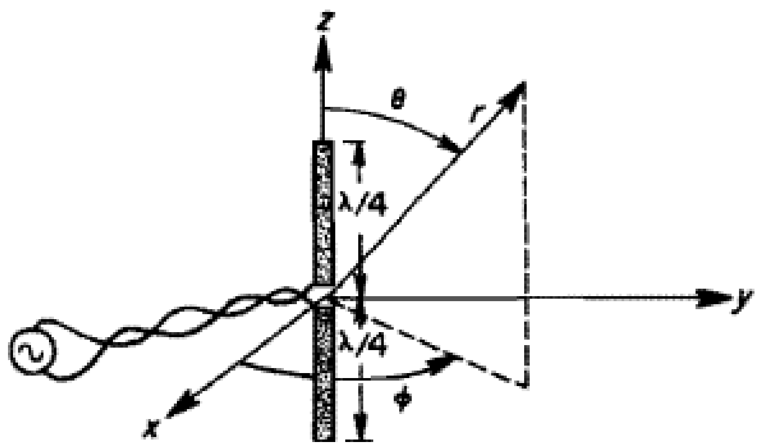

Figure 4: A center-fed half-wave dipole i.e. total length from end to end is λ/2. [*Reproduced from Lines, Waves, And Antennas: The Transmission of Electric Energy*].

While the input impedance of a half-wave dipole at resonance can be easily matched to a 50 Ω transmission line, its physical size can be several meters long; thereby rendering it impractical for the frequency range of interest (VHF-UHF). The antenna size is then reduced such that it becomes "electrically small" i.e. $l < \lambda/20$ [27] where l is the length of an arm of the dipole or its radiation power factor is much below unity [28]. Radiation factor is the ratio of the radiated power to reactive power. Although an electrically-small antenna offers the apparent physical size benefit, it is an inefficient radiator of energy. In fact, due to its highly reactive impedance component, it is basically a storage element (capacitor) as shown in Fig. A.1 and A.3 of Appendix A. Consider a straight dipole antenna in Figure 4 with a resonant frequency of 238 MHz; at 10 MHz, the electrical length of the 60 cm-long antenna is $\lambda/50$. The input impedance is -j3.4 kΩ. [The magnitude of the resistive component of the impedance was too small to measure with the vector network analyzer]. Given its low input resistance, the conventional dipole antenna would not be suitable as a transmit antenna. However, if a broadband antenna could be designed to excite multiple resonances, one of which could be optimized to yield sufficiently low return loss at a frequency of interest in the VHF-UHF region, then this antenna would be an appropriate transmitter for a VHF-UHF application. Examples of such types of antennas are considered next.

4. Characterization of Meander Dipole Antennas

Meander antennas generally offer size reduction and broadband benefits. Therefore, they are typically used for wireless communications [29], [30] and Radio-frequency identification (RFID) applications [31]. The frequencies of these applications are typically in the upper UHF-microwave spectrum. Therefore, meander antennas for applications lower than UHF, and with a low-profile, had not been widely considered.

Meander dipole antennas are a special case of dipole antennas in that, a conventional dipole antenna is a meander dipole antenna with zero bends. There were broadband equivalent circuits presented in the following references with varying degrees of accuracy: [32], [33], [34], and [39]. Accuracy of the model is usually enhanced either by adding more lumped elements i.e. RLC branches [18] or by an adaptation of a genetic optimization algorithm [31] to optimize the lumped element values to a particular network topology. However, accuracy improvements come at an added cost of increased complexity. Relative to a conventional dipole antenna, a meander dipole possesses the advantage of increased physical and electrical length and bandwidth for a given height.

Analysis of meander antennas was needed to determine the effect of the number of bends effect on return loss. It is also important to examine how the resistance, inductance, and capacitance are affected with the introduction of meander sections in a wire antenna.

Developing an equivalent model for a meander antenna which accurately predicts its self-resonant frequency is an ongoing work. Few approaches such as the inductor circuit model [35] and the Transmission Line Model [36] have been proposed. In the inductor circuit model representation, the resonant frequency of a meander-line antenna was determined from the self and mutual inductances of the wire, which were expressed as a function of wavelength. As a result, the self-capacitance of the wire was ignored. In addition, the model was inherently narrowband. Best concluded in [37] that the inductive circuit model was not adaptive to variations in the meander section spacing when estimating the resonant frequency. The approach presented by Puente *et al* [36], which was based on the transmission line model, was also narrowband and did not provide an intuitive method for calculation the resonant frequency of meander-line antennas.

4.1 The Three-bend Meander Dipole Antenna

A three-bend Meander Dipole Antenna (MDA) was chosen for further study. Figure 5 shows the MDA with a straight-wire dipole antenna. Both dipoles had been constructed with an 18-gauge copper wire. The straight-wire monopole is 30 cm long (physical length) while the MDA monopole dimensions are as follows: 30 cm (physical size) and 55.71 cm (i.e. the total length including the horizontal segments). Warnagiris and Minardo [38] stated that meandering an antenna into the same physical size as a straight-wire dipole antenna yields a much lower resonance frequency than the straight-wire antenna; a claim that has been verified through simulation and measurements (see Fig. 6). The "calc" curves in Figure 6 were generated by adapting equations for lumped element parameters for a straight dipole model presented in [39] to an MDA. The adaptation procedure will be discussed in S*ections 4.2* and *4.3*. With a baseband frequency of 1.5 MHz (from the DDA-AM application in *Chapter 2*), the electrical length of the MDA is $\lambda/180$. The calculated radiation resistance (R_r) and radiation efficiency (η_r) for the antenna are 24.4 mΩ and 18.4 % respectively. While these values are still small, they represent improvements of 334x for R_r and 6.1x for η_r over the previous antenna used in evaluating the performance of the DDA.

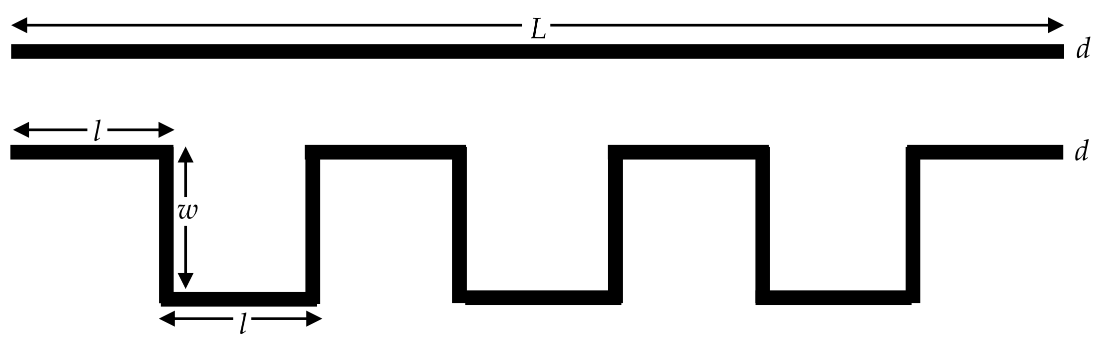

(a)

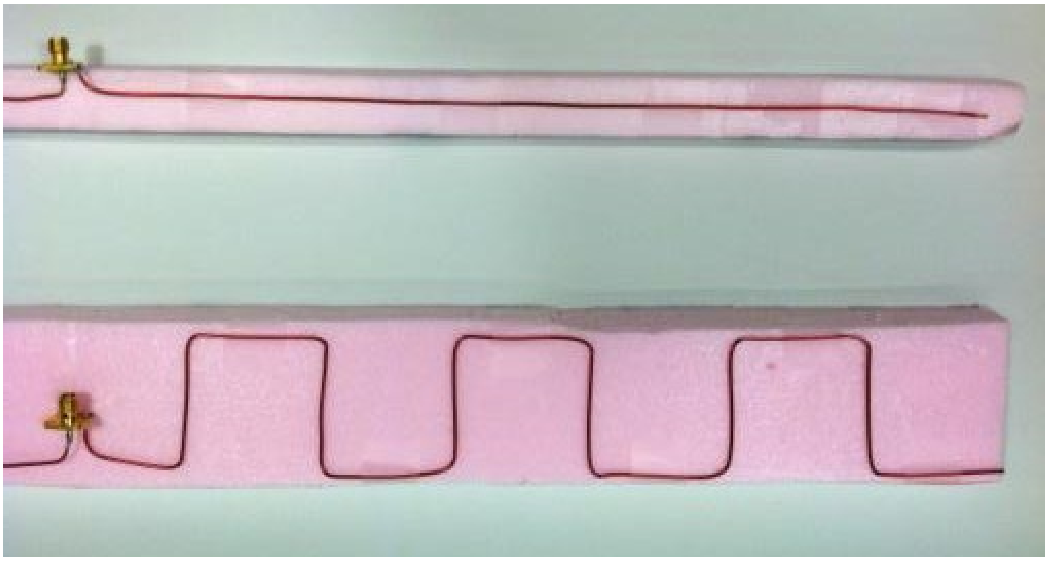

(b)

Figure 5: Cross-sectional view of Meander and Straight (Quarter-wave) dipole antennas (single-arm). (a) A Two-dimensional drawing and (b) A prototype. In (a), L = 30 cm, l = w = 4.3 cm, d = 0.105 cm.

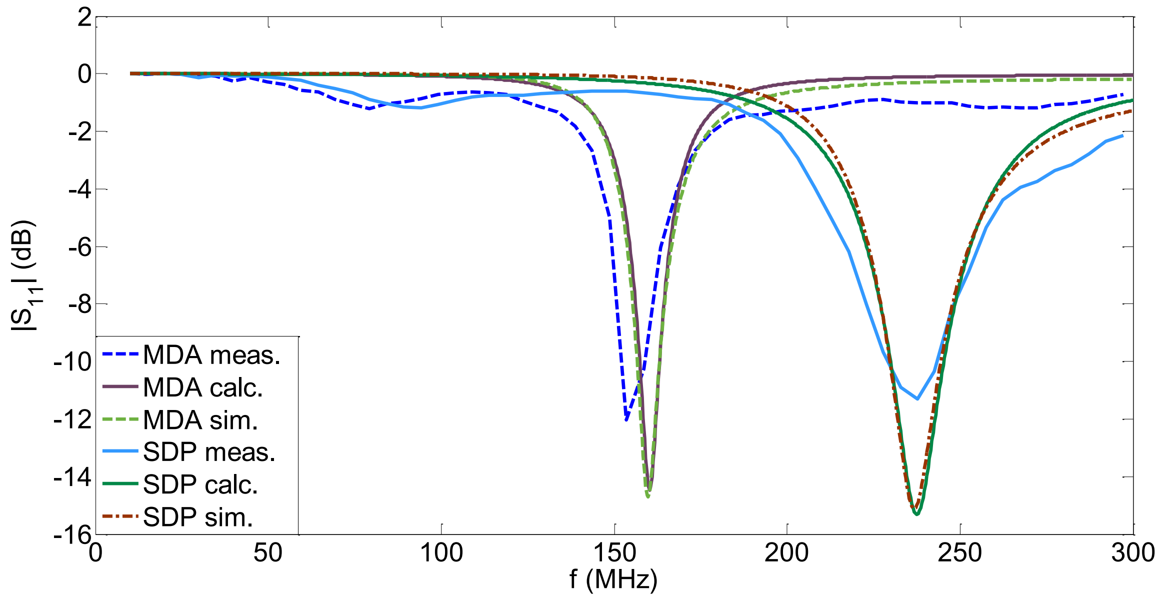

Figure 6: Overlay of the return losses of the antennas in Fig. 5. MDA - Meander Dipole Antenna, SDP - Straight Dipole Antenna. Note: the "calc." curves were derived from Multisim [51] SPICE simulation of the adapted MDA model. The lumped element parameters in the adapted MDA model come from the revised set of equations in (2a-2c). The "sim." curves from EMCoS simulation, while the "meas." curves are Network Analyzer measurements.

4.2 Analysis of Meander Dipole Antennas using a Frequency-Independent Lumped –Element Model

Further theoretical analysis of meander dipole antennas in general was performed via the introduction two newly-defined classes: Class-1 and Class-2. For a Class-1 MDA, the total length of the wire l_0 or L is kept constant. As each meander is introduced, the mutual capacitance in each meander section increases while the overall capacitance in the antenna structure decreases because of the mutual capacitances in adjacent meander sections that combine in series. As the number of bends increases, the overall capacitance of the antenna decreases while the inductance of the wire remains constant for a Class-1 MDA, a consistent increase in the resonant frequency of the antenna was observed with increasing N for a Class-1 MDA.

Figure 7 shows a series of meander dipole antennas (single arm) with different bends and their return losses as computed by EMCoS [40] in Figure 8. A shift in the S_{11} curves from left to right implies that the antenna appears increasingly shorter electrically as expected with addition of bends and the impedance match relative to a 50 Ω feed point varies, with N = 2 or 3 providing the best match.

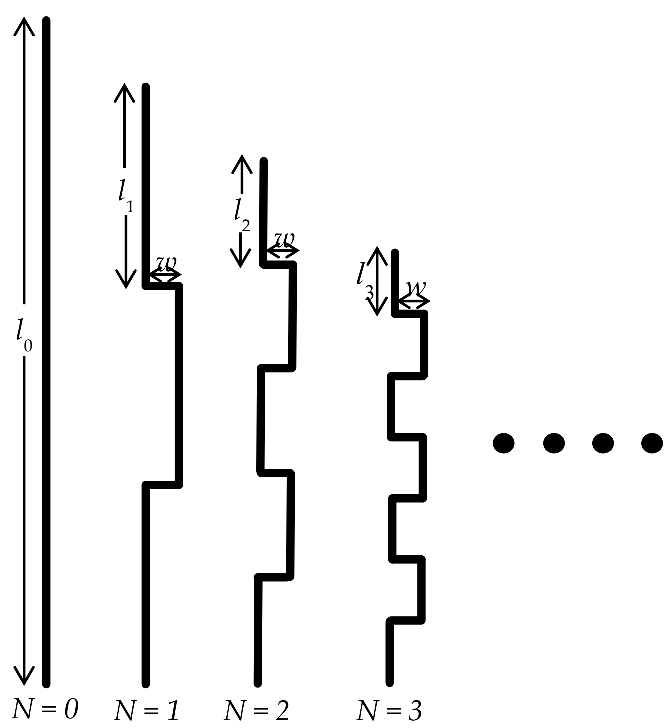

Figure 7: Single-arm Class-1 MDA. N = 0 to 8, $l_0 = L$ = 1 m, w = 0.05 m. The total length (vertical and horizontal segments) of each N configuration equals l_0.

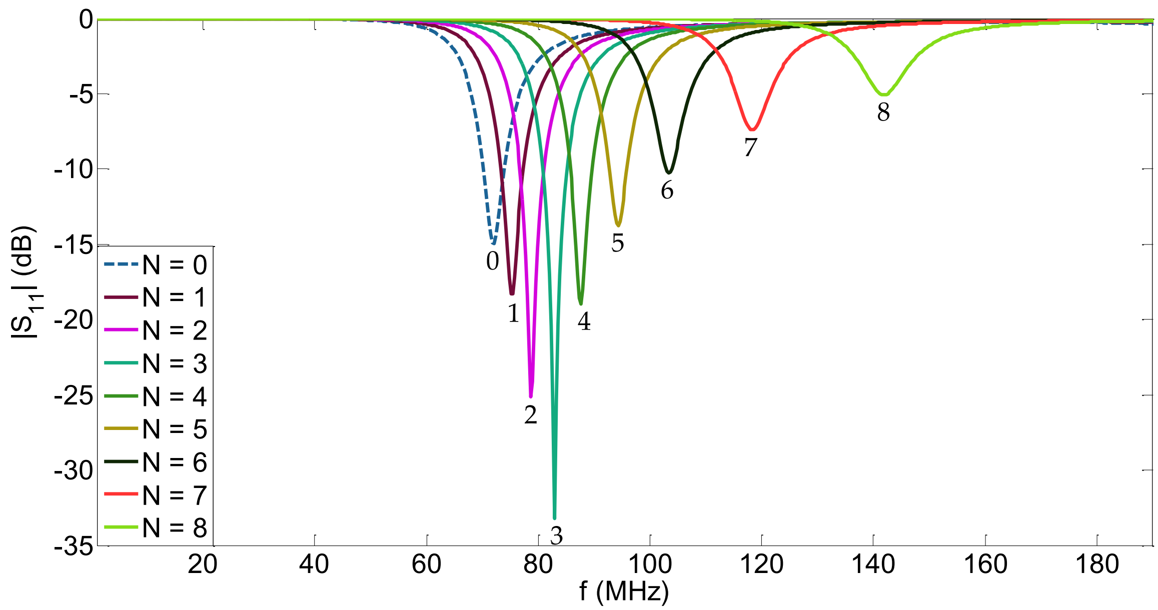

Figure 8: EMCoS Antenna Virtual Lab simulation of Class 1 meander dipole antennas with multiple bends. The numbers on the plot represent the number of bends for each corresponding curve.

For a Class-2 MDA, the height l_0 of the antennas remain fixed while the total length of the wire increases as more bends are added. As the length of wire increases, so does the total inductance. Although adding bends has a similar effect on the overall capacitance as described for a Class-1 MDA, the increase in inductance dominates, and for a Class-2 MDA, consistent decrease in the resonant frequency of the antenna was observed with increasing N.

Figure 9 shows a series of Class-2 meander dipole antennas (single arm) with different bends and their return losses as computed by EMCoS [40] in Figure 10. Based on the shift of the return loss curves from right to left in Figure 10, it can be observed that the antenna appears increasingly longer electrically as expected with addition of bends and the impedance match relative to a 50 Ω feed varies, with N = 1 or 2 providing an acceptable match.

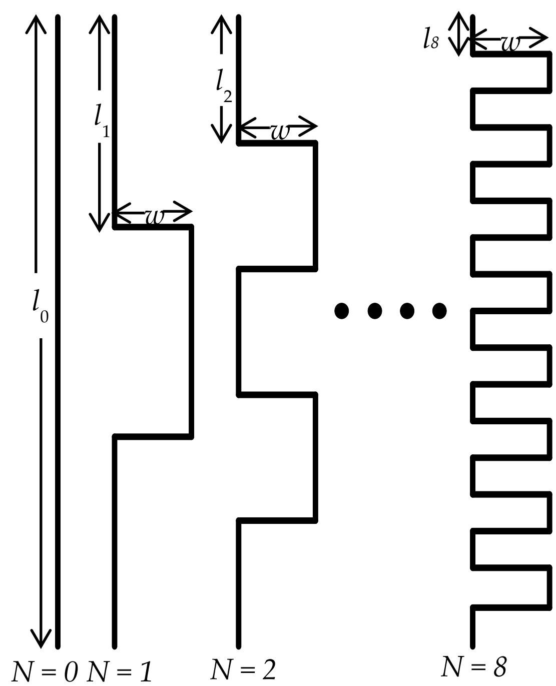

Figure 9: Single-arm Class 2 MDA. N = 0 to 8, $l_0 = L$ = 0.3 m, w = 0.05 m.

Meander dipole antennas were modeled and characterized previously by Endo et al [35]. In [35], a center-fed meander dipole antenna was decomposed into short-terminated transmission line sections. Each section was modeled with lumped elements (inductors) and analyzed with transmission-line equations. The resonant frequency of an MDA was predicted from the equation of the total inductance i.e. self and mutual inductance of the antenna wire. Best and Morrow [37] concluded that the inductive circuit representation of meander antennas, which does not account for the capacitance of the meander sections, is inaccurate in predicting the resonant frequency and is not versatile with geometrical changes in the antenna. The difference between the approach described here and the others mentioned previously is that the MDA model presented here, which is an adaptation of the half-wave dipole model presented in [39], consists of lumped elements that are entirely a function of the antenna geometry rather than frequency, an approach that is inherently more broadband and more accommodating of changes in geometry and configuration.

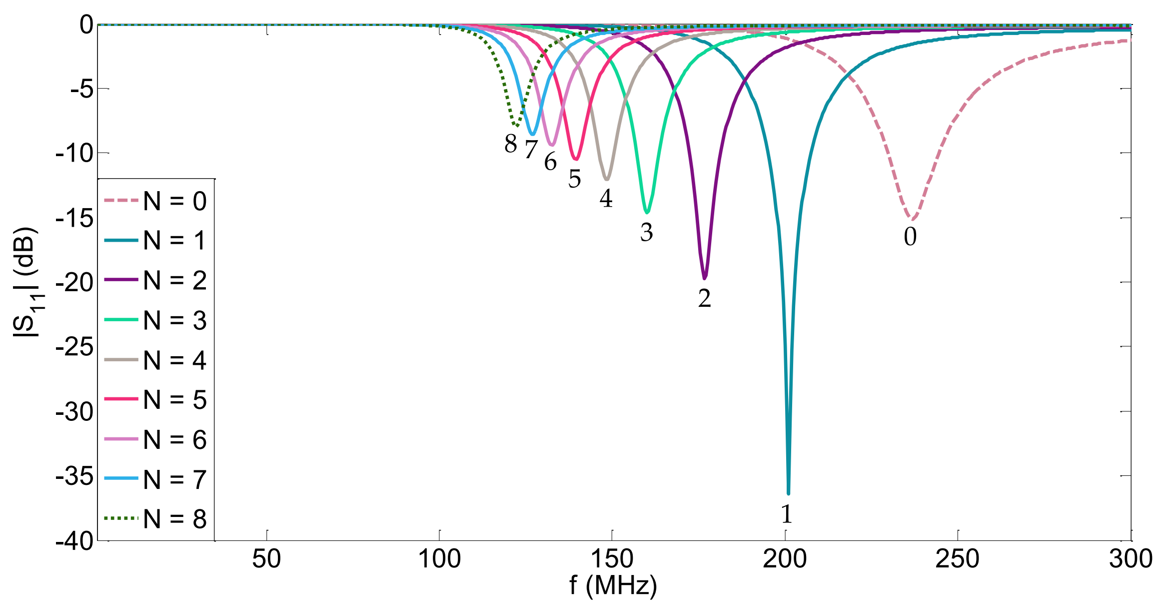

Figure 10: EMCoS Antenna Vlab simulation of Class 2 meander dipole antennas with multiple bends. The numbers on the plot represent the number of bends for each corresponding curve.

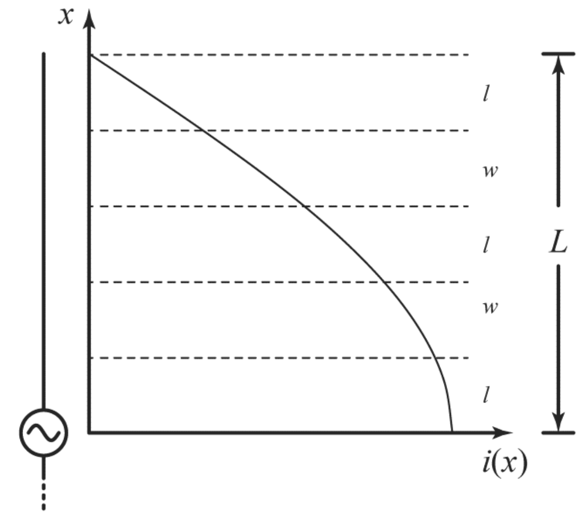

(a)

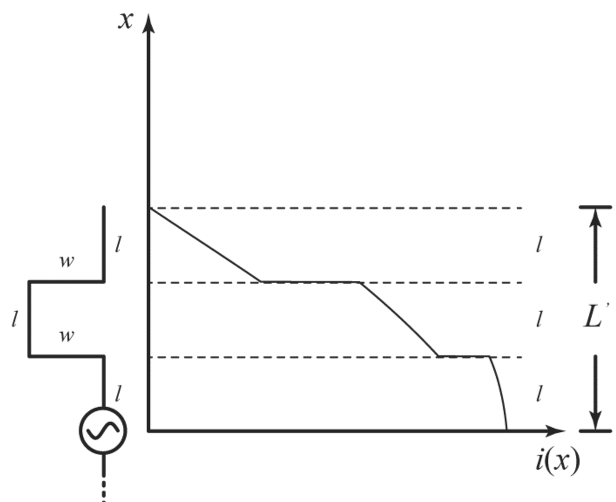

(b)

Figure 11: Current distributions on one-half of: (a) A Straight Dipole Antenna and (b) A Meander Dipole Antenna. The regular cosine current distribution on the straight monopole becomes a piecewise distribution on the meander monopole (ideally) due to the lack of contribution from the bent (*w*) segments.

4.3 Theoretical Analysis of the Meander Dipole Antenna Model

A Meander Dipole Antenna (MDA) has many similarities to its straight dipole counterpart. Nakano [41] found the radiation patterns to be similar. As illustrated in Fig. 11, currents on adjacent horizontal segments are opposite in direction and the spacing between them are much smaller than wavelength; thus, ideally canceling their currents [42] and yielding negligible radiation on the horizontal segments[43]. As a result, the current distribution on the meander dipole is a piecewise representation of the current distribution on the Straight Dipole Antenna (SDP) wire. These similarities will be exploited later to derive a frequency-independent, geometry-based MDA model.

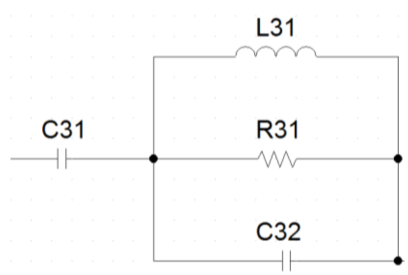

Figure 12: Broadband equivalent circuit model from [8] used for both the SDP and the MDA.

Tang et al [39] derived a four-element model (see Fig. 12) for a straight dipole antenna. The equations to calculate all the lumped elements were a function of the antenna geometry. Based on the MDA-SDP similarities identified previously, these equations can be adapted to MDAs as well. The lumped element equations in [39] have been reproduced in (2a-2c) in their original forms. Modifications of the equations for the MDA model have also presented in (3a-3c) below.

$$C_{31} = \left\{\frac{12.0674h}{log\left(\frac{2h}{a}\right)-0.7245}\right\} pF \tag{2a}$$

$$C_{32} = 2h\left\{\frac{0.89075}{\left[log\left(\frac{2h}{a}\right)\right]^{0.8006}-0.861} - \ 0.02541\right\} pF \tag{2b}$$

$$L_{31} = 0.2h\left\{\left[1.4813 \ log\left(\frac{2h}{a}\right)\right]^{1.012} - 0.6188\right\} \mu H \tag{2c}$$

$$C_{31} = \left\{\frac{12.0674(L-2wN)}{log\left(\frac{2(L-2wN)}{a}\right)-0.7245}\right\} pF \tag{3a}$$

$$C_{32} = 2(L - 2wN)\left\{\frac{0.89075}{\left[log\left(\frac{2(L-2wN)}{a}\right)\right]^{0.8006}-0.861} - \ 0.02541\right\} pF \tag{3b}$$

$$L_{31} = 0.2L\left\{\left[1.4813 \ log\left(\frac{2L}{a}\right)\right]^{1.012} - 0.6188\right\} \mu H \tag{3c}$$

where N is the number of bends, *a* is the radius of the wire, w is the length of the horizontal segment, and *L* is the total wire length of each arm of the MDA. In Fig. 13, $L = (7l + 6w)$. The equations for C_{31} and C_{32} do not consider the horizontal segments of the MDA while the equation for L_{31} does. The self-inductance of a wire remains relatively unchanged as long as the length of the horizontal segment, *w* is electrically small. Therefore, L_{31} is approximately equal to the self-inductance of a straight dipole given in

[39]. The bending of the wire introduces mutual capacitances between the adjacent wire segments that constitute a meander section. The mutual capacitance of a meander section is:

$$C_m = \frac{\pi\epsilon_0 w}{ln\left[\frac{l_S}{a}+\sqrt{\left(\frac{l_S}{a}\right)^2-1}\right]} \tag{4}$$

where l_S is the spacing between two parallel wires that form a meander section, w is the width of the section and a is the radius of the wire.

$$l_S = \frac{(l-2wN)}{2(2N-1)} \tag{5}$$

Therefore, the resonant frequency, f_0 of an MDA can be predicted as follows:

$$f_0 = \frac{1}{2\pi\sqrt{L_{31}\left(C_{31}+C_{32}+\frac{Cm}{2(2N-1)}\right)}} \tag{6}$$

where N is the number of bends.

A wire with a fixed length L = 100 cm, width w = 4.3 cm, and radius, a = 0.0525 cm was chosen. Varying the number of bends, N in a Class-1 MDA from 0 to 8 and comparing predictions of the resonant frequencies from (6) and [35] with numerical simulations in EMCoS [40], the result in Fig. 14 was obtained. In comparing both predictions accurately, it is worth noting that a bend is defined differently in this document than in [35], but there is a correlation given in (7). Let N' represent the number of bends in an MDA as defined in [17] and N be the number of bends as defined in this document. Therefore, N' is related to N by:

$$N' = 2N - 1 \tag{7}$$

The width of a section, w is defined the same way in both manuscripts. In Fig. 15, there was a good agreement between both models considered and the simulation results from N = 3 to 7 but a divergence could be observed below $N = 3$ and above $N = 7$. The largest deviations from simulation results of the MDA model and [35] were 2.3% and 9.8%, respectively.

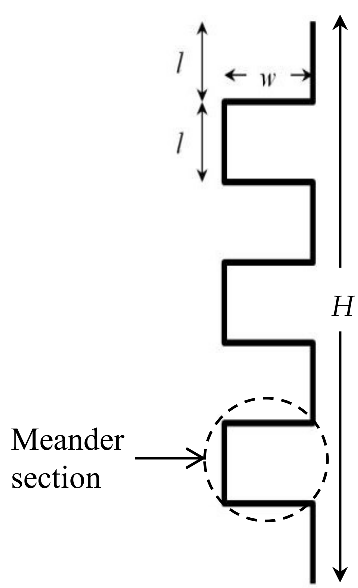

Figure 13: One arm of a three-bend (N = 3) MDA. The total length of one arm of the wire is L i.e. $L = (7l + 6w)$. H is the height. For each N considered, the lengths of all vertical segments, l are equal. The lengths of all horizontal segments, w are also equal.

Similarly, for a Class-2 MDA, the height, H of each arm of the MDA was fixed at 30 cm while w = 4.3 cm. The number of bends was again varied from 0 to 8. Resonant frequency predictions of the MDA model (6) and the inductive-circuit model [35] were compared with EMCoS simulation values and presented in Fig. 15. There was a good agreement between both models with EMCoS simulation results for N = 2 and above. For N = 2 and below, the inductive-circuit model [35] deviated substantially, by up to 28% at N = 0. The largest deviation observed between the model and simulation results was 3.4%.

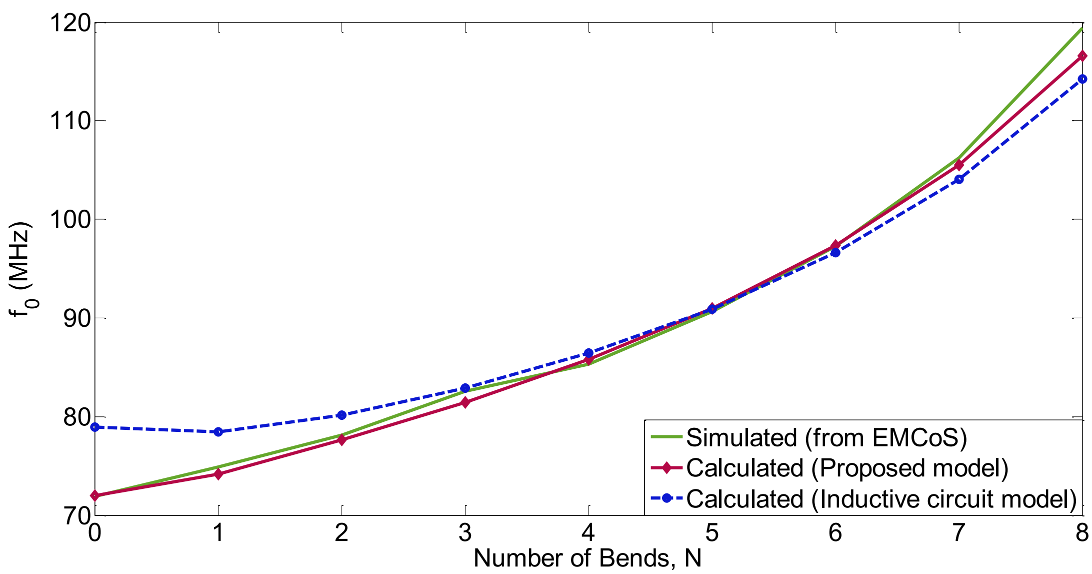

Figure 14: Class-1 MDA. Resonant frequency, f_0 as a function of the number of bends in one arm. Plot compares the results from numerical simulation in EMCoS with both predictions from the frequency-independent, geometry-based MDA (proposed) model and the inductive circuit model. The length of the wire, L = 100 cm, width, w = 4.3 cm.

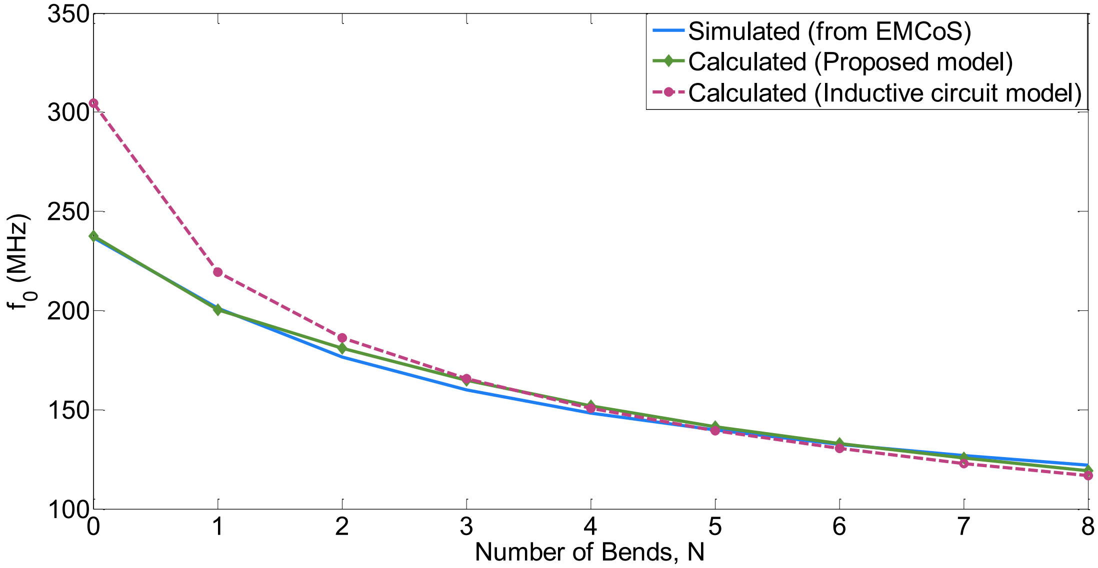

Figure 15: Class-2 MDA. Resonant frequency, f_0 as a function of the number of bends in one arm. Plot compares the results from numerical simulation in EMCoS with both predictions from the frequency-independent, geometry-based MDA (proposed) model and the inductive circuit model. The height of the antenna above the ground plane, H = 30 cm, width, w = 4.3 cm.

4.3.1 Radiation Resistance

The radiation resistance of an antenna is an integral part of characterizing the antenna in terms of its performance and efficiency. Therefore, we present an equation for estimating the resonant frequency of the MDA, which is a function of the geometry and frequency. This method considers the vertical segments of the MDA such as that shown in Fig. 3 as its main radiating elements [44]. The input resistance of an MDA is given by:

$$R_{in} = 34.15\left(\pi\frac{(L-2wN)}{\lambda}\right)^{1.8} \tag{8}$$

where L is the total length i.e. both vertical and horizontal segments of each arm of the MDA, w is the width, and N is the number of bends. The input resistance equation (8) was modeled after input resistance equations of dipoles in [11] but with the constants adapted to the MDA configuration. Assuming ohmic losses are negligible, the input resistance is the radiation resistance. An overlay of predicted radiation resistances on the values obtained via EMCoS [40] are contained in Fig. 16.

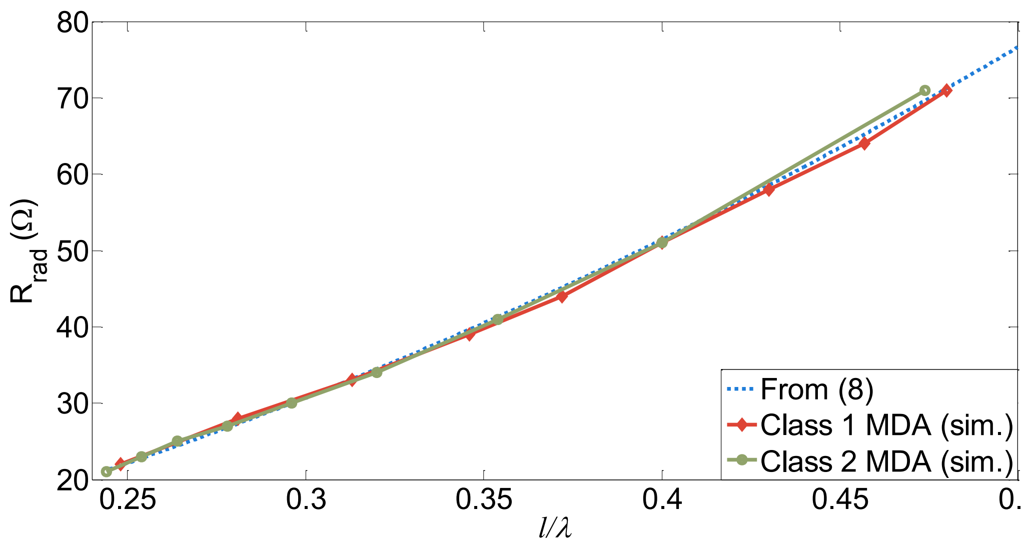

Figure 16: Class-1 and Class-2 radiation resistances as a function of wavelength and predictions by (8). "sim." indicates that data was obtained by simulation in EMCoS.

4.3.2 Sensitivity Analysis

Given that multiple factors influence the prediction of the resonant frequency and the radiation resistance of a Meander Dipole Antenna, analyses of the effects of the variables in the resonant frequency and radiation resistance equations for a Meander Dipole Antenna were conducted. The effects can be determined from the rate of change (or the partial derivative) of the independent variable of concern relative to the dependent variable. The sensitivity curve of the radiation resistance equation of (8) was obtained by the following:

$$\delta R_{rad} = \frac{\delta R_{in}}{\delta\left(\frac{l}{\lambda}\right)} \tag{9}$$

Where $l = L - 2wN$ and it represents the total rise or the sum of all the vertical segments of the MDA. $\delta R_{rad}/\delta(l/\lambda)$ was then plotted against l/λ as shown in Fig. 17. Over the range of 0.25λ to 0.5λ, the rate of change of the radiation resistance of the MDA is directly proportional to the rate of change of the electrical length of the vertical, radiating segments.

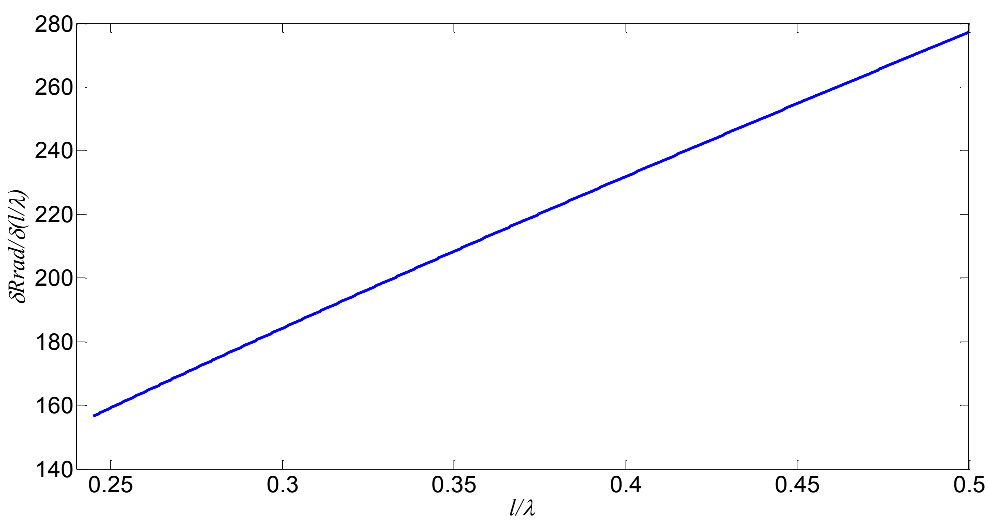

Figure 17: Sensitivity of the Radiation resistance curve to the electrical length (*l*/λ).

Similarly, sensitivity analyses of the resonant frequency of the MDA with respect to the total length of the wire, *L* and the number of turns, *N* were performed separately by taking the partial derivative of f_0 in (6) with respect to *N* and *L*, respectively. This is in contrast to the sensitivity analysis of the radiation resistance whereby the cumulative length of the vertical segments is the most important. In this case, *N* and *L* variables influence the resonant frequency calculations. The results are presented in Figures 18 and 19. In Fig. 18, we observe that the rate of change of f_0 varies over the range of $0 \leq l \leq 1$ m with f_0 being very sensitive between $l \sim 0.22$ m but as is expected, increasing the overall length of the wire reaches a point where f_0 is no longer sensitive to the additional lengths as shown in the $l > 0.33$ m. The data range below $\delta f_0/\delta l < 0$ has been ignored due to its lack of practical significance.

In Fig. 19, the sensitivity of the resonant frequency curve varies with the frequency of operation (f) of the antenna. The rate of change of f_0 relative to *N* increases at higher frequencies. Because of consistency in the data trend, plots for only one decade (f = 10 - 100 MHz) is shown. The result in Fig. 19 assumes that the widths of all turns are the same and are fixed at a particular value and that the length of each arm of the MDA is 0.25 λ.

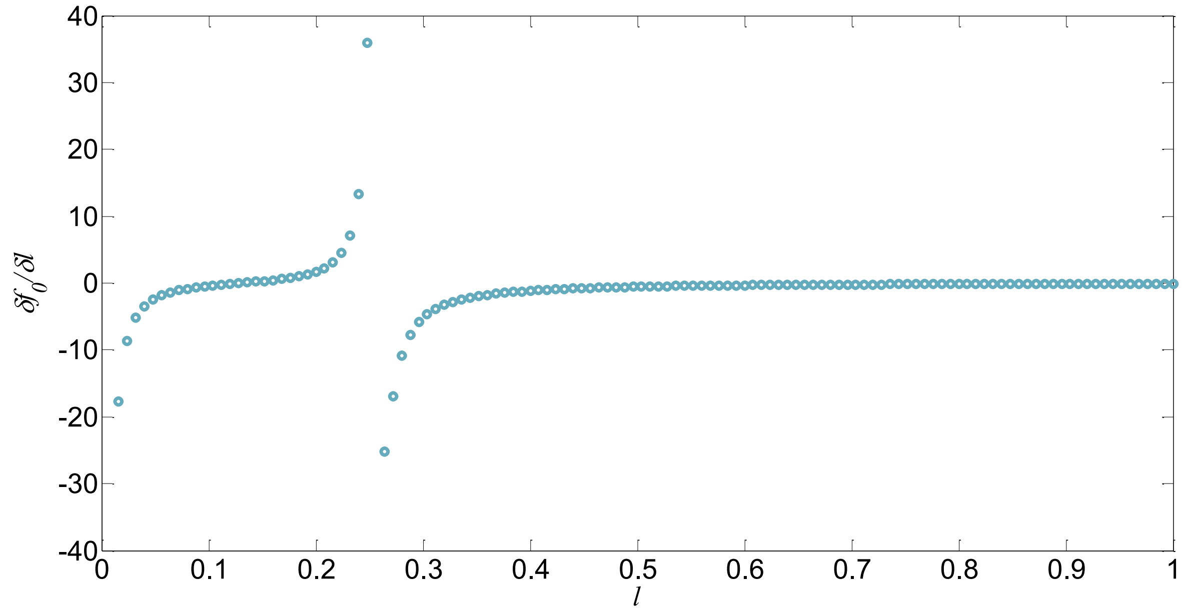

Figure 18: Sensitivity of the resonant frequency curve to the physical length, *l* (in m).

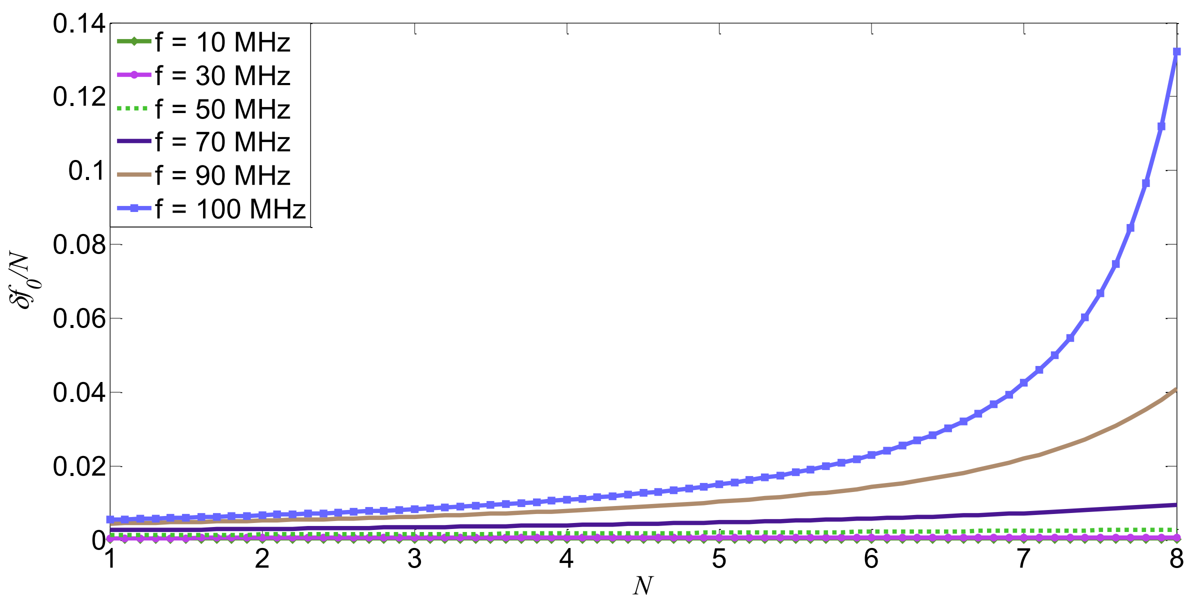

Figure 19: Sensitivity of the resonant frequency curve to the number of turns, *N*.

5. Meander – Spiral Antenna Equivalence

Another broadband wire antenna with a higher radiation resistance that will be investigated for low-profile, small-footprint applications is the spiral or helical antenna, used interchangeably to refer to the same type of antennas within the context of this dissertation. Compared to a short monopole, we know from published literature that the radiation resistance of spiral antennas (normal mode) is typically 1.62x higher [11] (10), (11). Relative to meander antennas, spiral antennas possess the added advantage of confining physically longer wires in a smaller space, and are broadband. Conventional spiral antennas come in different configurations: monofilar [12], [13], [15], bifilar [14], [15], quadrifilar [16], [17], and octafilar [18]. They are used in applications such as Global Positioning System-enabled devices [19], [20], satellite communication equipment [21], [25], and RFID readers [22] [26]. Although, many turns of a helical antenna can be ideally confined in a small space, in practice, the antenna wires require winding around a cavity for structural support, which grows its form factor. Few attempts had been made to implement some form of meandering to an existing helical antenna design [23], [24] in order to achieve size reduction. However, a cavity is still required for structural support. The series of spirals (or helical) antennas analyzed here replaces the cavity with layers of dielectric materials with electrical properties as close to air as possible (see Figure 24 (b) for a sample illustration).

$$R_r \approx 640 \left(\frac{h}{\lambda}\right)^2 \Omega \quad \textit{normal mode helix antenna} \tag{10}$$

$$R_r = 395 \left(\frac{h}{\lambda}\right)^2 \Omega \quad \textit{short monopole antenna} \tag{11}$$

where h is the height of the monopole and helix antennas and λ is the wavelength.

There are two configurations of the "spiral" antenna presented: the normal mode spiral antenna, which has been widely studied and the "reverse-wound" spiral, which is a novel concept; both are shown in Figs. 20 (a) and (b), respectively. The spiral antennas in Figure 20 were inspired by the alternate representation of helical antennas as a series of loops of wires interconnected with straight wires presented in [44]. A meander antenna can be derived from a reverse-wound spiral antenna via an "unfolding" process shown in Fig. 21. Therefore, existing models or procedures used to optimize the meander dipole described in *Chapter 4* could also be applicable to spiral antennas. The normal and reverse-wound spirals were numerically analyzed by EMCoS [40] to compare the effect of the different winding directions of both antennas on the return loss at resonance. In Figure 22, it was observed that both configurations in Figure 20 resonated at slightly different frequencies but the configuration in Figure 20 (b) yielded a lower return loss at resonance. Since Figure 20 (b) is clearly a more desirable configuration, its return loss was compared with that of its MDA equivalent antenna obtained as shown in Figure 23. According to Figure 23, there was good agreement between the return loss data of the spiral antenna in Figure 20 (b) and its MDA equivalent in relation to their resonant frequencies. At the main resonance point, the difference in the frequencies was 5 MHz. Note that since a spiral antenna is usually constructed over a ground plane, one arm or the meander dipole antenna was also positioned on the ground plane in the simulation environment to ensure an accurate comparison of both antennas.

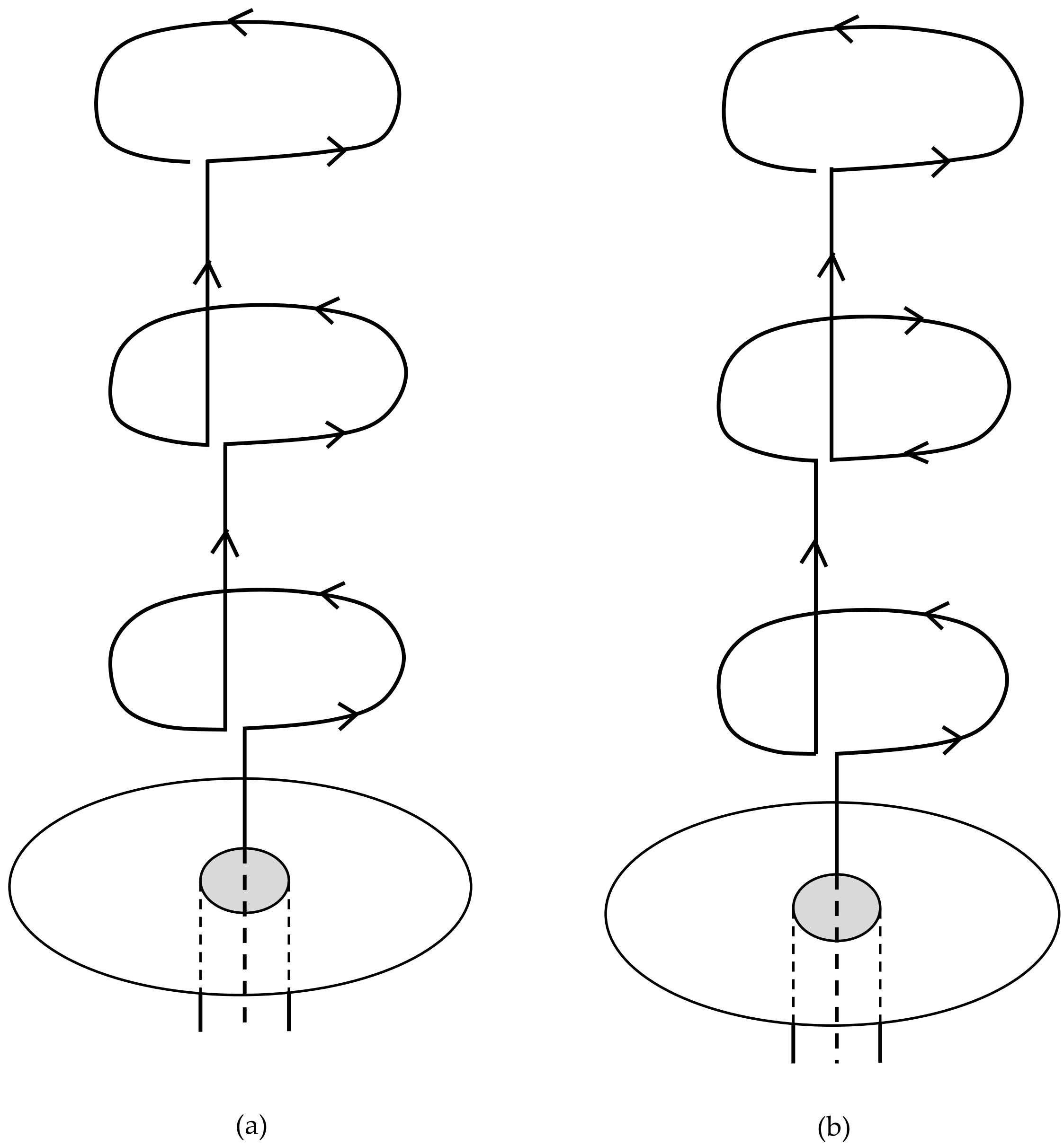

Figure 20: Alternate winding directions of a helical antenna. (a) Forward-wound spiral antenna configuration: Currents in adjacent loops are in the same direction. (b) Reverse-wound spiral antenna configuration: currents in adjacent loops are in opposite directions. Arrows represent the direction of current flow.

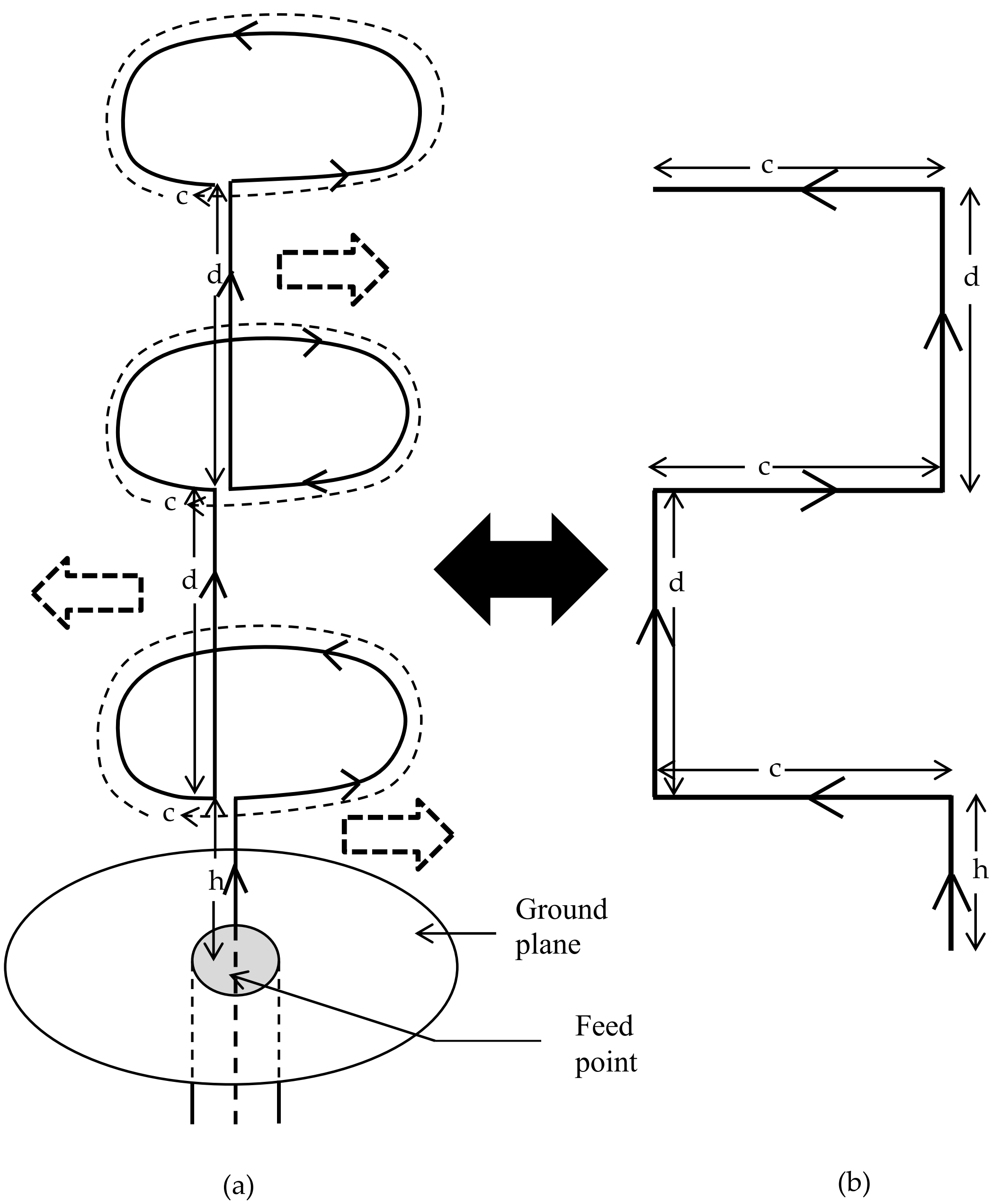

Figure 21: Structural equivalence of the reverse spiral and a meander line antenna. (a) A spiral antenna. (b) A conventional meander monopole antenna equivalent. Segments *h* and *d* are displaced in the direction of the dotted block arrows to obtain (b). The arrows on the wires represent the direction of current flow. The reverse spiral is equivalent to a meander line antenna while the forward spiral is not.

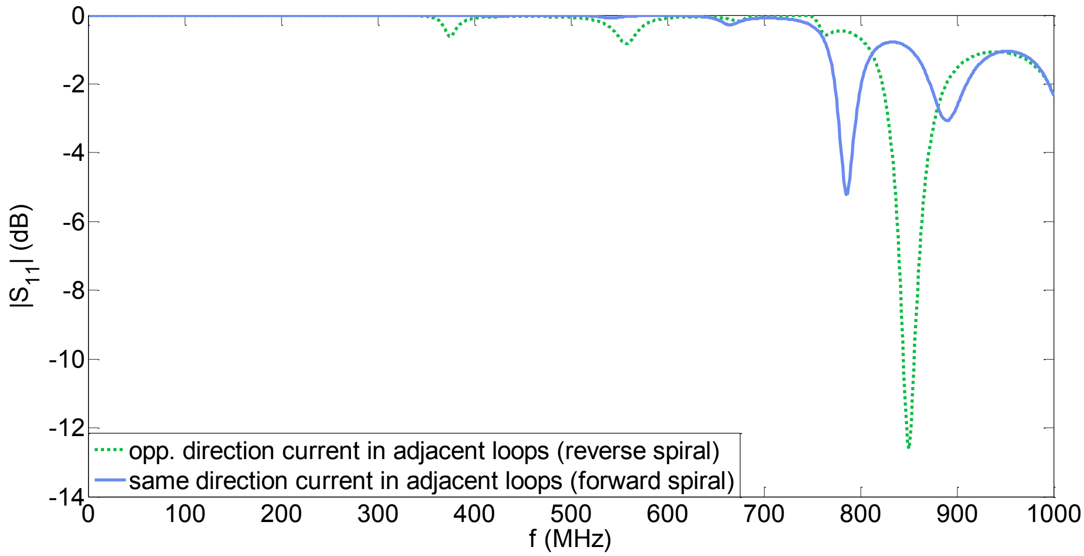

Figure 22: Return loss (in dB) curves of the forward wire-based and reverse wire-based spiral antennas in Figure 20.

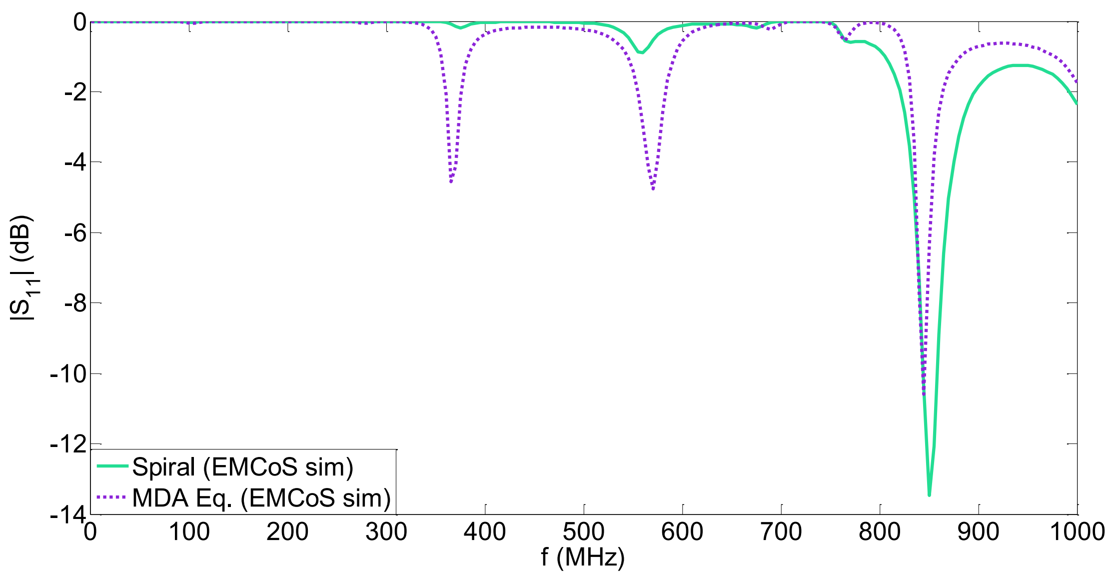

Figure 23: Return loss (in dB) curves of the reverse spiral antenna in Figure 20 (b) and its MDA equivalent.

The reverse-wound spiral antenna shown in Figure 24 illustrates its compactness. It consists of a continuous wire looped four times and stacked in layers of Plexiglas (εr ~2.6-3.5) slabs as structural support. For simulation purposes, εr = 3.1 was assumed. The entire structure was mounted on a 24″ x 24″ ground plane. Each loop is 10 cm in diameter.

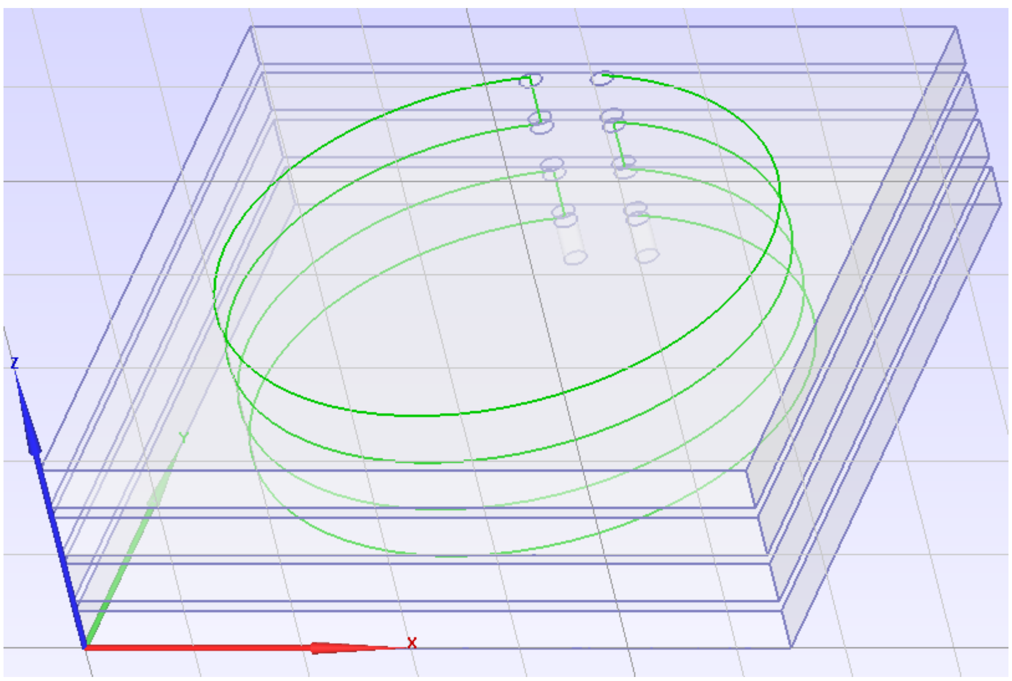

(a)

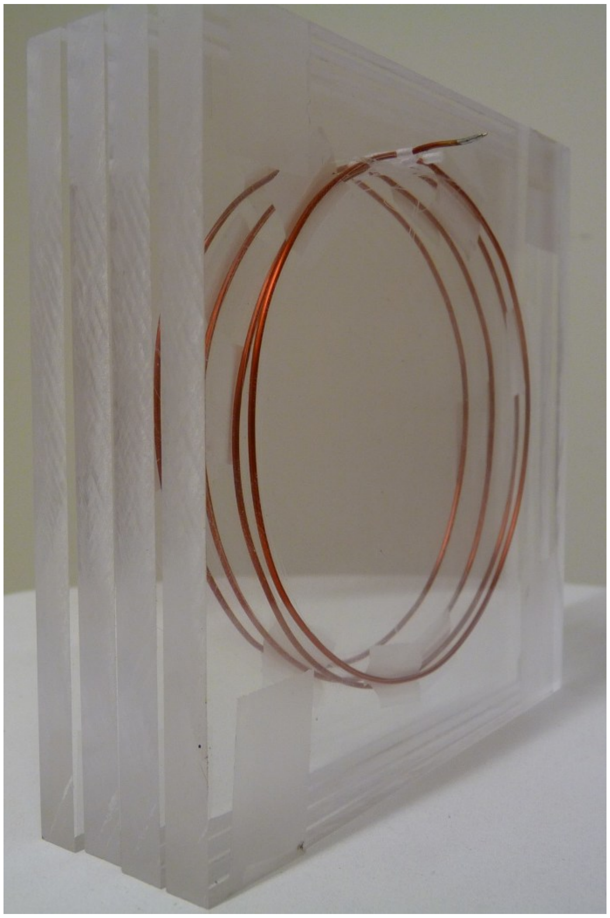

(b)

Figure 24: Prototype of the reverse-wound spiral. (a) A Three-dimensional model and (b) A prototype. A continuous wire is formed into four loops with diameter of 10 cm on Plexiglas (ε_r = 2.6-3.1) slabs.

5.1 Stripline Meander Antenna

A new form of antenna that combines both spiral and meander antenna characteristics is introduced. It is called the Stripline Meander Antenna (see Figure 25). In a stripline meander antenna, wires have been replaced with metallic or Perfect

Electric Conductor (PEC) strips. Similar analyses to the wire-based, forward- and reverse-wound spiral antennas were performed on these antenna configurations in FEKO [45], a Moment-Method electromagnetic field solver. The aim of these analyses was to repeat the investigation of the effect of an antenna winding on its frequency response. A series of numerical simulations of the antenna models shown in Figure 25 were performed in FEKO [45]. Each model was positioned on an infinite ground plane that is not shown in the figures. The models were then excited with a 1 V source and the return loss results shown in Figure 26. Each antenna model simulated excited multiple resonances, which is consistent with the broadband nature of conventional spiral antennas. In the 900 MHz region i.e. the region where the return loss is at least the minimum acceptable level of 15 dB, the percentage of incident power will be reflected by the forward stripline spiral antenna was 3% at 909 MHz while only 0.2% incident power will be reflected by the reverse stripline spiral antenna at 917 MHz. Therefore, the reverse spiral configuration offers a significant improvement over the forward spiral configuration at identical frequencies, which is a similar trend to the behavior of wire-based spiral models previously observed. The stripline antennas offer significant profile reductions as well. For example, the height reduction obtained from the reverse stripline spiral antenna would be ~52% at 917 MHz relative to a half-wave dipole at the same frequency.

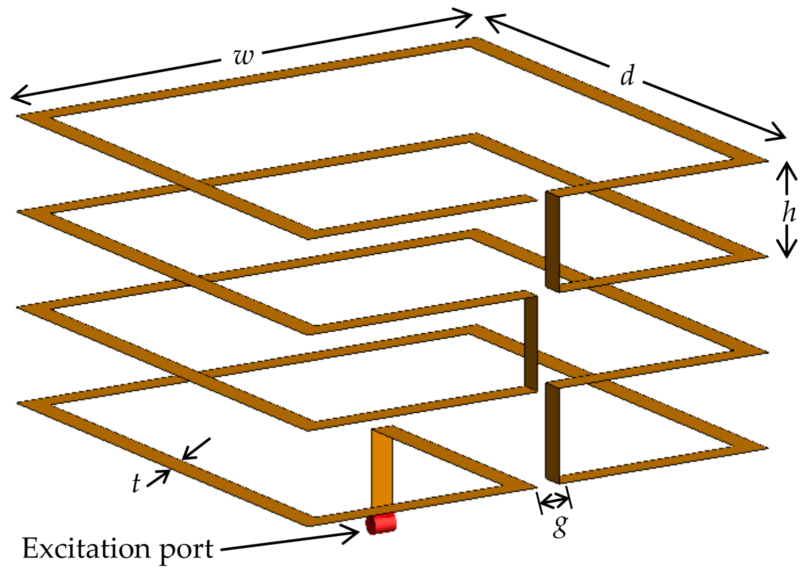

(a)

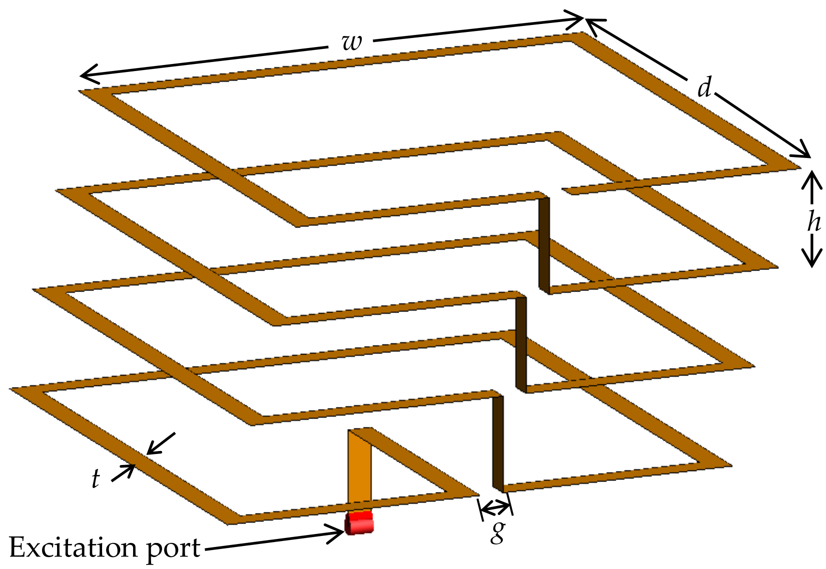

(b)

Figure 25: Stripline meander antennas models. (a) Reverse-wound stripline spiral. (b) Forward-wound stripline spiral. w = d = 0.1 m, t = g = 0.005 m, h = 0.02 m.

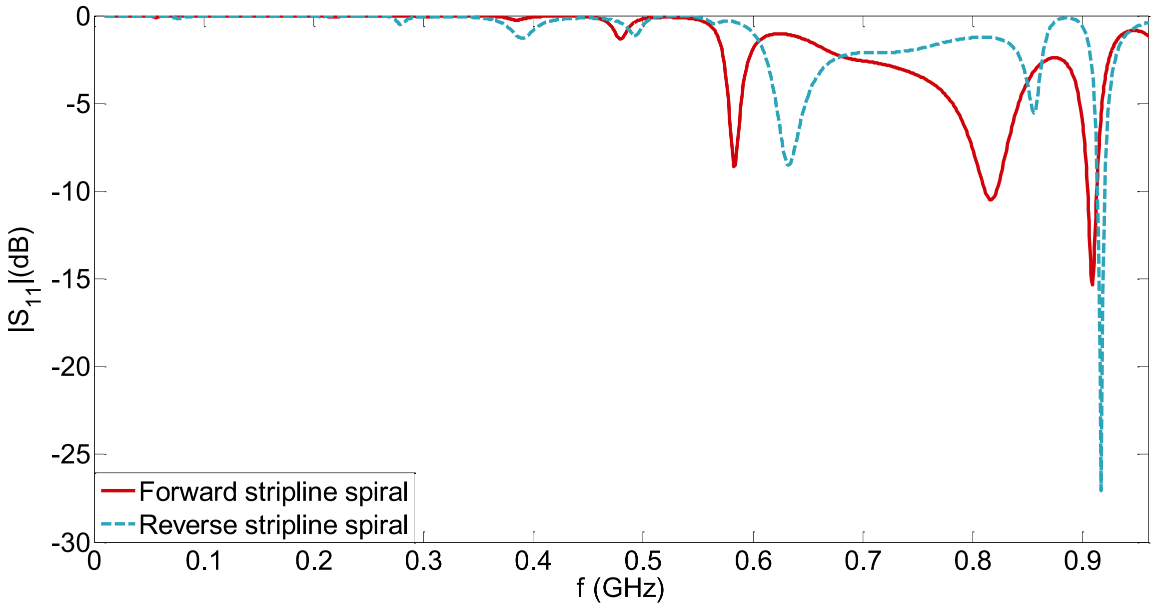

Figure 26: Overlay of the return loss plots of the forward and reverse stripline antenna.

5.2 Bowtie Meander Dipole Antenna

Bowtie antennas have been known to be physically small, compact and broadband, which are desirable features for an antenna in low-frequency applications. Bowtie meander antennas were studied in [46] and [47]. Ali and Stuchly [46] found that a monopole bowtie meander antenna yields a 39-55 % length reduction over a monopole meander antenna. Also, for the same electrical length, a meander bowtie antenna has a larger input resistance relative to the meander antenna. However, the Bowtie MDA analyzed in this section is of a different configuration from the previously studied MDA and may be geometrically equivalent to another type of spiral antenna.

The geometric equivalence between the Bowtie MDA and the Reverse-wound spiral was investigated. A graphical illustration of this equivalence is shown in Figure 27. Each corresponding segment has an identical label i.e. the horizontal segments of Bowtie MDA correspond to the loops on the spiral antenna while the vertical segments of both antennas are identical. Unlike the regular MDA-spiral case (see Fig. 21), the result of the numerical analysis of Figure 27 with the dimensions in Figure 29 revealed inconsistences between the return loss data of both structures (see Figure 28). The closest agreement occurred at the fundamental resonant frequencies of both antennas. A possible explanation for this observation is that the simulation tool was unable to accurately estimate the fringing capacitance between successive bends of the Bowtie MDA, which will not be insignificant due to the unequal lengths of the parallel segments.

A Bowtie MDA in Fig. 27 was modeled, analyzed, prototyped, and measured using the following dimensions; the length of the smallest horizontal segment x is 3 cm and every subsequent horizontal segment is an integer multiple of x up to $8x$. The length of each vertical segment y is 6 cm. In Figure 30, there were multiple resonances excited, including at low frequencies. For example, the return loss of the Bowtie antenna at 64 MHz is 15 dB. Therefore, it is possible to obtain a good match to a 50 Ω source at a frequency as low as 64 MHz with an antenna that is less than 1 m tall. This antenna represents a 55% height reduction relative to a half-wave dipole antenna that resonates at the same frequency.

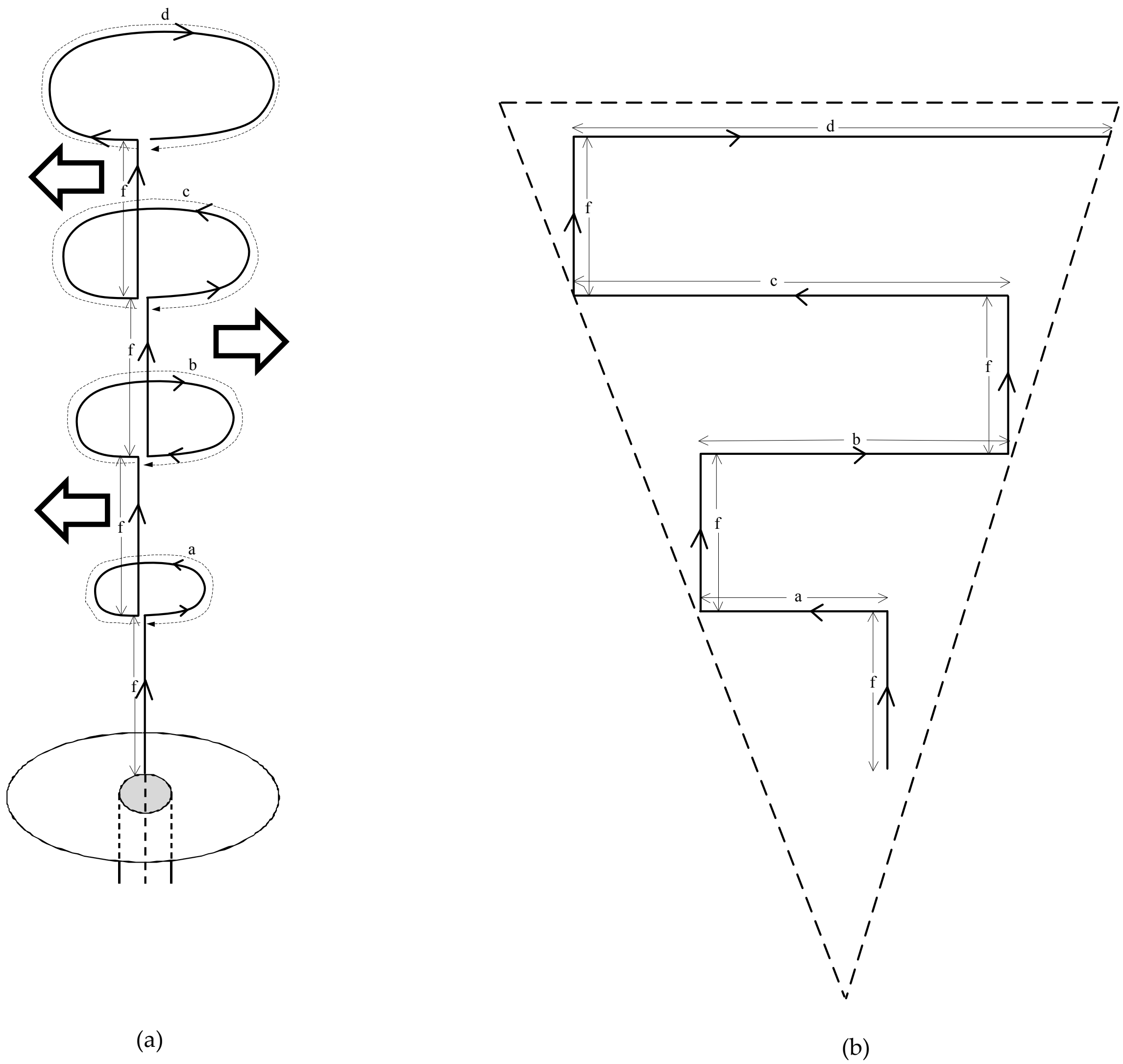

Figure 27: Structural equivalent of spiral and bowtie antennas. (a) A reverse-wound spiral antenna and (b) A bowtie meander dipole antenna equivalent. The vertical segments labeled *f* are displaced in the direction of the block arrows to obtain (b). The arrows on the wires represent the direction of current flow.

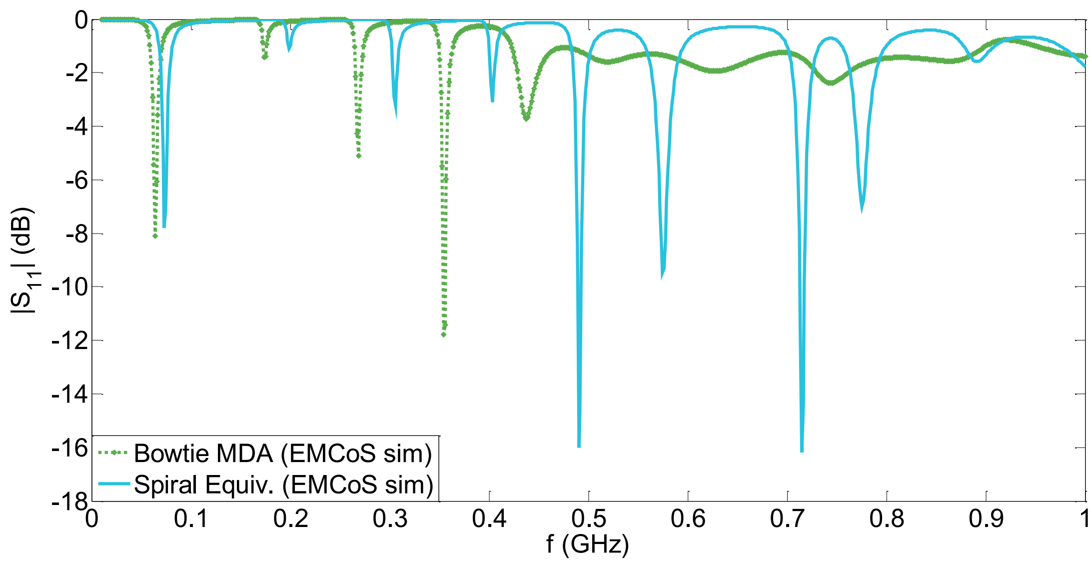

Figure 28: Bowtie MDA-Spiral geometric equivalence analysis in EMCoS.

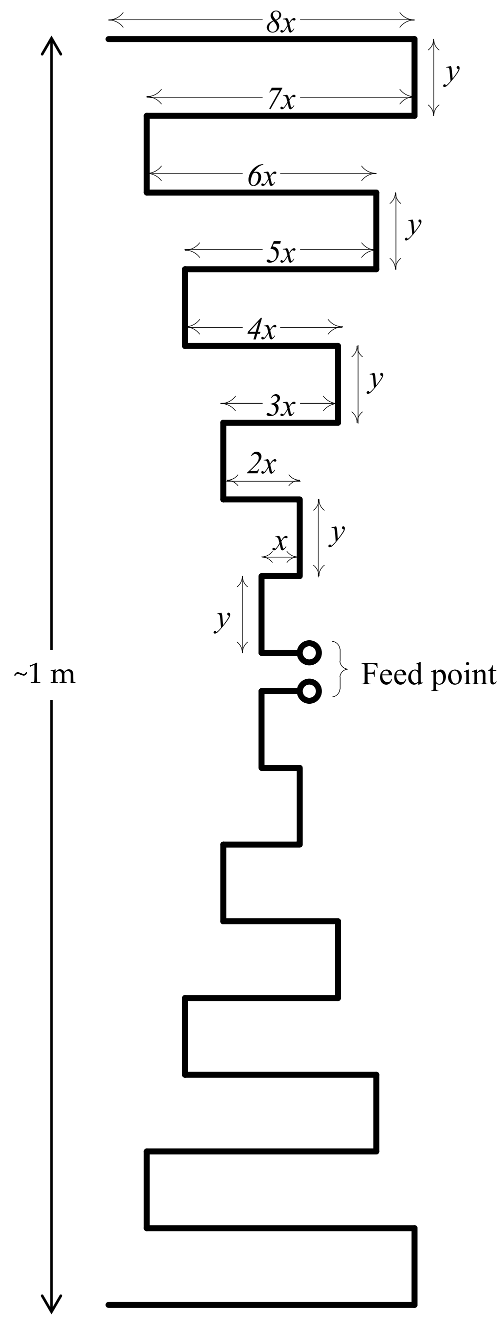

Figure 29: Sketch of the Modeled and Prototyped Bowtie MDA. The antenna is center fed via a 50 Ω source. x = 3 cm, y = 6 cm. Total length of wire used including both horizontal and vertical segments = 3.12 m.

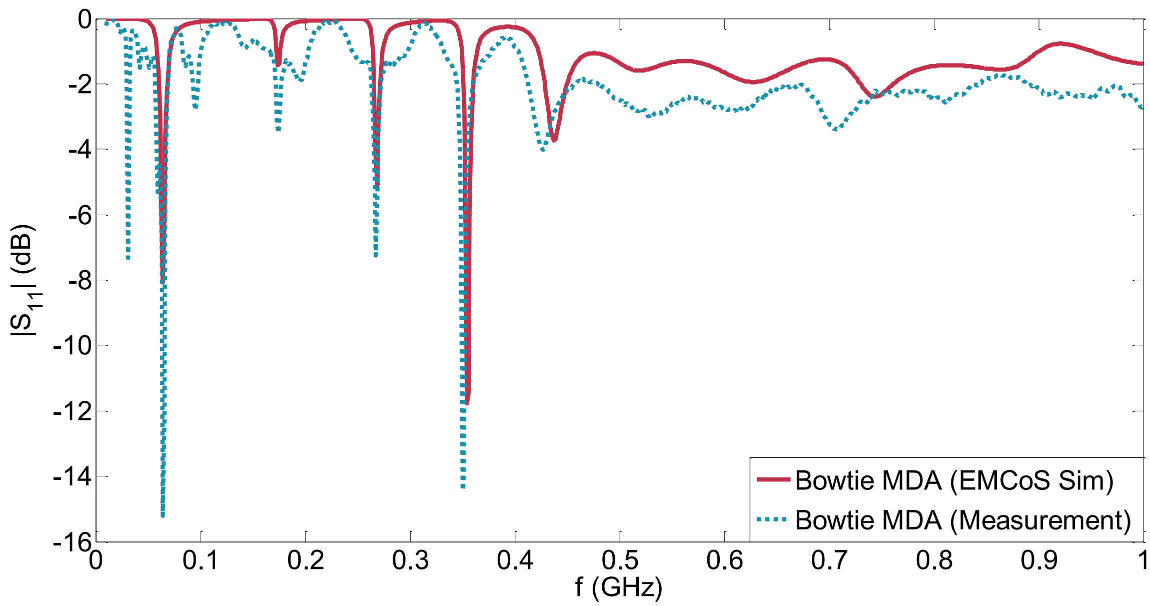

Figure 30: Return loss curves (in dB) of the Bowtie Meander Dipole Antenna (MDA). The "EMCoS Sim" curve was obtained via the EMCoS numerical analysis software while the "Measurement" curve was obtained from the constructed prototype in an anechoic chamber.

6. Conclusion

Briefly stated, these are my original contributions: 1. In this dissertation I have explored and enhanced the desirable characteristics of meander-line and helical (or "spiral") antennas at microwave frequencies in the UHF-VHF bands. For example, it was discovered in this work that the reverse-spiral antenna had a unique and predictable operating frequency, but the forward-spiral antenna had multiple smaller resonances, none of which were desirable. 2. I have also proposed and developed novel antenna geometries that combine spiral and meander-line properties and have analyzed their performance. These antennas offer significant size reductions; for example, a bowtie meander dipole antenna studied yielded a height reduction of 55% at 64 MHz relative to a half-wave dipole antenna for the same resonant frequency. 3. I have also developed and presented a new and improved set of design equations for predicting the resonant frequency and radiation resistance of meander-line antennas. The body of work presented here has been featured in several peer-reviewed publications. They can be found in the *Biography* section.

The dissertation has explored a wide-ranging set of topics; from proposing an alternative transmitter architecture for the Directly-Driven Antenna application to finding a suitable antenna for low-frequency applications such as the DDA, given size (low-profile, small-footprint) and frequency (VHF-UHF range) constraints. The alternative transmitter was prototyped and tested at AM frequencies and was found to be more efficient over the conventional AM transmitter design; although this observation was made with an electrically small i.e. total length ~ $\lambda/3300$ and very inefficient dipole antenna (See Appendix B). Given that the antenna could be longer but still remain within an acceptable size limit, other electrically longer antenna configurations were investigated. They are: half-wave dipole, meander (regular and bowtie), wire-based spiral (forward and reverse-wound) antennas, and stripline spiral (forward and reverse-wound) antennas. An analytical procedure for estimating the resonant frequencies and the radiation resistances of meander antennas was determined. During the course of my investigations, a geometric correlation between the spiral and the conventional meander antenna was confirmed using return loss data, although the correlation between the bowtie meander antenna and its geometric spiral equivalent was inconclusive. Any geometric correlation between two antenna types suggests that the procedures used to analyze one antenna type could be adapted to another antenna type. A change in configuration of the spiral antennas from forward- to reverse-wound changed the resonant frequencies and the values of S_{11} at resonance, but not the number of harmonics. This suggests that the reverse-wound configuration would be a more desirable configuration for a practical application.

The results from the prototype bowtie MDA simulation suggests that an antenna can be well-matched to a 50 Ω source at a low frequency of 64 MHz and at a height of 1 m because only 3.2% [48] of the incident power on the antenna is reflected at this frequency. A total height of 1 m for the Bowtie MDA represents a 55% reduction in height relative to a half-wave dipole at equal resonant frequency. Similarly, the reverse-wound stripline antenna featured in this work yielded a 52% profile reduction at 917 MHz. A return loss of 15 dB or higher is a reliable indicator of good impedance match; thus, is a widely-acceptable standard for antenna design in the industry.

Appendix A

Meander Antenna Optimization: A Graphical Approach

A different approach to modeling a meander dipole antenna by its R, L, and C components is a graphical procedure inspired by Brown et al [1]. In [1], a series of Reactance vs. electrical length curves were generated for a straight-line, cylindrical dipole antenna of various diameters (as a function of wavelength) as shown in Fig. A.1. Through a reactance-electrical length and a resistance-electrical length curve, the feed-point radiation resistance of a dipole antenna as well as its R-L-C parameters could be determined. Joines [49] demonstrated this approach for a standard straight-line, center-fed dipole antenna.

The standard dipole was represented with the equivalent circuit in Fig. A.2. First, a series combination of R_{rad}, L_S and C_S was selected to represent a straight-line dipole antenna. For a given antenna diameter relative to wavelength (r_0/λ) curve in Fig. A.1, this model appeared adequate in determining the reactance of the dipole in the linear region of the reactance-length curve around resonance but deviated towards the lower l/λ region. Adding a parallel L-C circuit that is resonant at the same frequency as the series L-C circuit corrected this deviation. Therefore, the radiation impedance Z_{RAD} was modeled with a parallel combination of L_S, C_S in series and L_P, C_P in parallel. Below is the derivation of the equations for the imaginary (X) and real (R) components of Z_{RAD}. The derivation has been reproduced here with permission.

The susceptance of the LC circuit in Fig. A.2 can be expressed as:

$$jB = j\omega C_P + \frac{1}{j\omega L_P} + \frac{1}{j\omega L_S + \frac{1}{j\omega C_S}} \tag{A.1}$$

At resonance,

$$\omega_0^2 = \frac{1}{C_P L_P} = \frac{1}{L_S C_S} \tag{A.2}$$

Factoring $\omega_0 C_P$ from the first two terms on the right of (A.1) and $\omega_0 L_S$ from the last set of the terms yields,

$$jB = j\omega_0 C_P \left(\frac{\omega}{\omega_0} - \frac{1}{\omega_0 C_P L_P}\right) + \frac{1}{j\omega_0 L_S\left(\frac{\omega}{\omega_0} - \frac{1}{\omega_0 L_S \omega C_S}\right)} \tag{A.3}$$

Substituting the ω_0 expression (A.2) in (A.3) yields,

$$jB = j\omega_0 C_P \left(\frac{\omega}{\omega_0} - \frac{\omega_0}{\omega}\right) + \frac{1}{j\omega_0 L_S\left(\frac{\omega}{\omega_0} - \frac{\omega_0}{\omega}\right)} \tag{A.4}$$

Alternatively,

$$jB = j\left[\omega_0 C_P \left(\frac{f}{f_0} - \frac{f_0}{f}\right) - \frac{1}{\omega_0 L_S\left(\frac{f}{f_0} - \frac{f_0}{f}\right)}\right] = j\left[\frac{\omega_0^2 C_P L_S\left(\frac{f}{f_0} - \frac{f_0}{f}\right)^2 - 1}{\omega_0 L_S\left(\frac{f}{f_0} - \frac{f_0}{f}\right)}\right] \tag{A.5}$$

And the reactance is,

$$jX = \frac{1}{jB} = j\left[\frac{\omega_0 L_S\left(\frac{f}{f_0}-\frac{f_0}{f}\right)}{1-\omega_O^2 C_P L_S\left(\frac{f}{f_0}-\frac{f_0}{f}\right)^2}\right] \tag{A.6}$$

Since the *R* vs. *l* curve in Fig. A.3 resembles an exponential function, the curve can be fitted with the following equation:

$$R = K_1 e^{(K_2 f/f_0)} \tag{A.7}$$

where K_1 and K_2 are constants.

Therefore,

$$Z_{RAD} = K_1 e^{(K_2 f/f_0)} + j\left[\frac{\omega_0 L_S\left(\frac{f}{f_0}-\frac{f_0}{f}\right)}{1-\omega_O^2 C_P L_S\left(\frac{f}{f_0}-\frac{f_0}{f}\right)^2}\right] \tag{A.8}$$

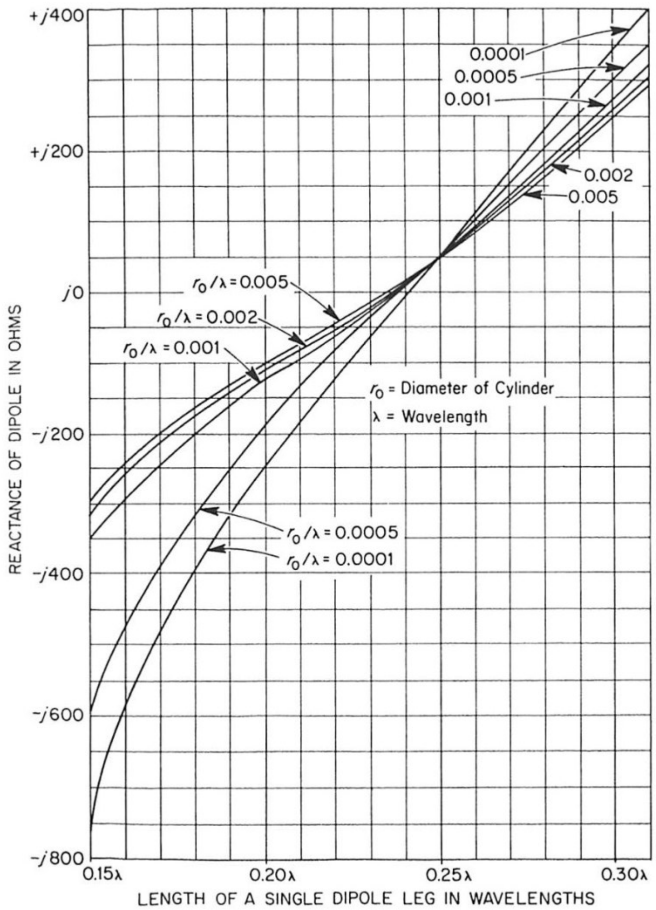

Figure 31: Reactance vs. Electrical length (single leg) of a Dipole. [*Courtesy: Lines, Waves, And Antennas book by R.G. Brown, R. A. Sharpe, W. L. Hughes, and R. E. Post*].

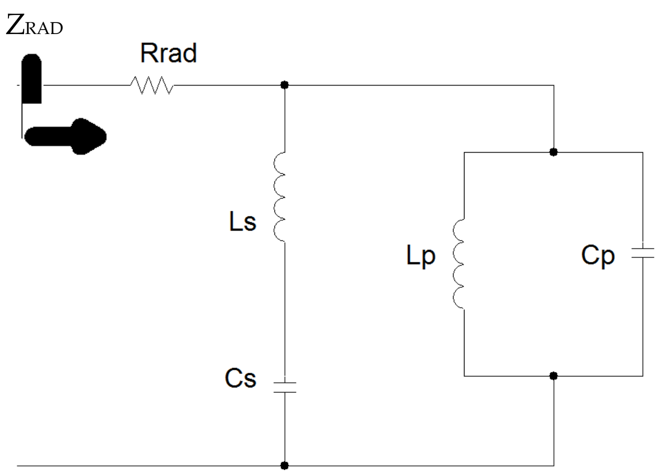

Figure 32: Equivalent circuit of a standard dipole antenna. [*Courtesy: Prof. William Joines, Duke University*].

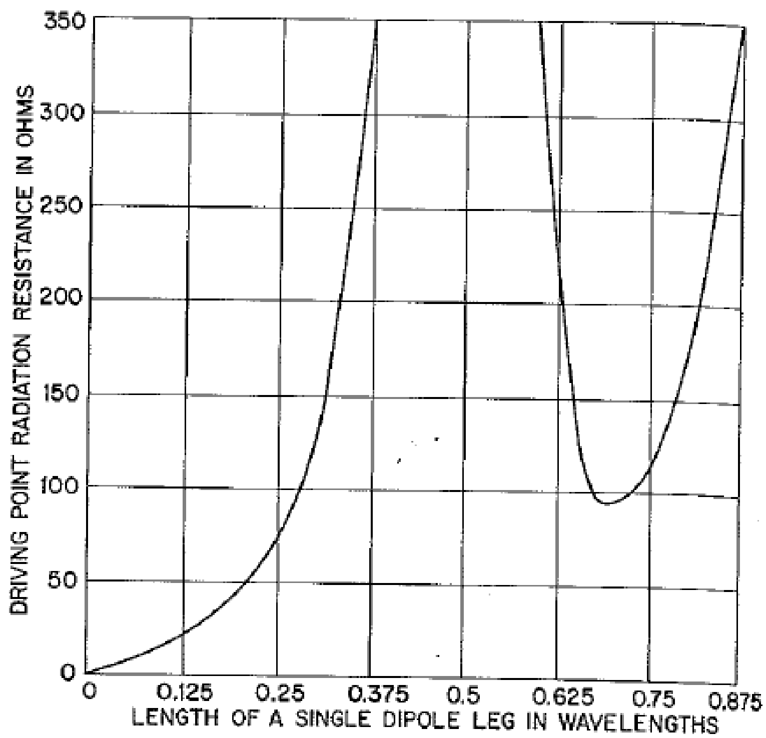

Figure 33: Resistance vs. Electrical length (single leg) of a dipole antenna. $l/\lambda \leq 0.375$ is the region of interest and can be modeled with an exponential function. [*Courtesy: Lines, Waves, And Antennas book by R. G. Brown, R. A. Sharpe, W. L. Hughes, and R. E. Post*].

The meander dipole antenna (MDA) in Fig. 4 was simulated in EMCoS [40], a commercially-available Moment Method solver. To generate the reactance- and resistance-length curves, the overall length (including the horizontal segments) of a single leg of the antenna was varied from 0.15λ to 0.35λ. Since the lengths of the horizontal segments were fixed at 4.3 cm each, consistent with the prototyped MDA in Fig. 4, the lengths of the vertical segments would vary from 0.15 λ to 0.35 λ. For each iteration of the electrical length, the input resistance, R and the input reactance, X were recorded at f = 160 MHz. The results were plotted as shown in Fig. A.4 and Fig. A.5, respectively. From Figure A.4, X = 0 at l_0 = 0.2841 λ. Since at resonance, the imaginary part of the impedance of an antenna is zero, l_0 = 0.2841 λ is the resonant electrical length. Two points on both sides of the X = 0 point on the X vs. l curve were selected.

Point 1: at l = 0.15λ, X = -984 Ω, $f/f_0 = l/l_0$ = 0.15/0.2841 = 0.528.

Point 2: at l = 0.1904λ, X = -494.1 Ω, $f/f_0 = l/l_0$ = 0.1904/0.2841 = 0.670.

Applying X and f/f_0 in (A.1), we have,

$$-j984 = j\left[\frac{\omega_0 L_S\left(0.528-\frac{1}{0.528}\right)}{1-(\omega_0 C_P)(\omega_0 L_S)\left(0.528-\frac{1}{0.528}\right)^2}\right] \quad \text{(A.9)}$$

$$-j494.1 = j\left[\frac{\omega_0 L_S\left(0.670-\frac{1}{0.670}\right)}{1-(\omega_0 C_P)(\omega_0 L_S)\left(0.670-\frac{1}{0.670}\right)^2}\right] \quad \text{(A.10)}$$

Solving (A.4) and (A.5) simultaneously, $\boldsymbol{\omega_0 C_S = 0.000231}$ **S** and $\boldsymbol{\omega_0 L_S = 549.537\ \Omega}$.

Similarly, if we choose two points on the *R* vs. *l* curve and fit the curve with an exponential function, K_1 and K_2 constants in (A.7) can be found.

Point 1: at $l = 0.16\ \lambda$, $R = 0.64\ \Omega$, $f/f_0 = l/l_0 = 0.16/0.2841 = 0.563$.

Point 2: at $l = 0.27\ \lambda$, $R = 22.4\ \Omega$, $f/f_0 = l/l_0 = 0.27/0.2841 = 0.950$.

Applying R and f/f_0 in (A.1), we have,

$$0.64 = K_1 e^{(K_2 \times 0.563)} \tag{A.11}$$

$$22.4 = K_1 e^{(K_2 \times 0.950)} \tag{A.12}$$

Solving (A.11) and (A.12) simultaneously, $\boldsymbol{K_1 = 0.00363}$ and $\boldsymbol{K_2 = 9.182}$.

Therefore, the complete equation for the radiation impedance, Z_{RAD} of the meander dipole antenna under consideration is:

$$Z_{RAD} = 0.00363 e^{9.182 f/f_0} + j \frac{549.537\left(\frac{f}{f_0} - \frac{f_0}{f}\right)}{1 - 0.127\left(\frac{f}{f_0} - \frac{f_0}{f}\right)^2} \tag{A.13}$$

The equation in (A.13) can be used to determine the radiation resistance of a MDA at a given frequency, provided the antenna has the same diameter as the one used in this study.

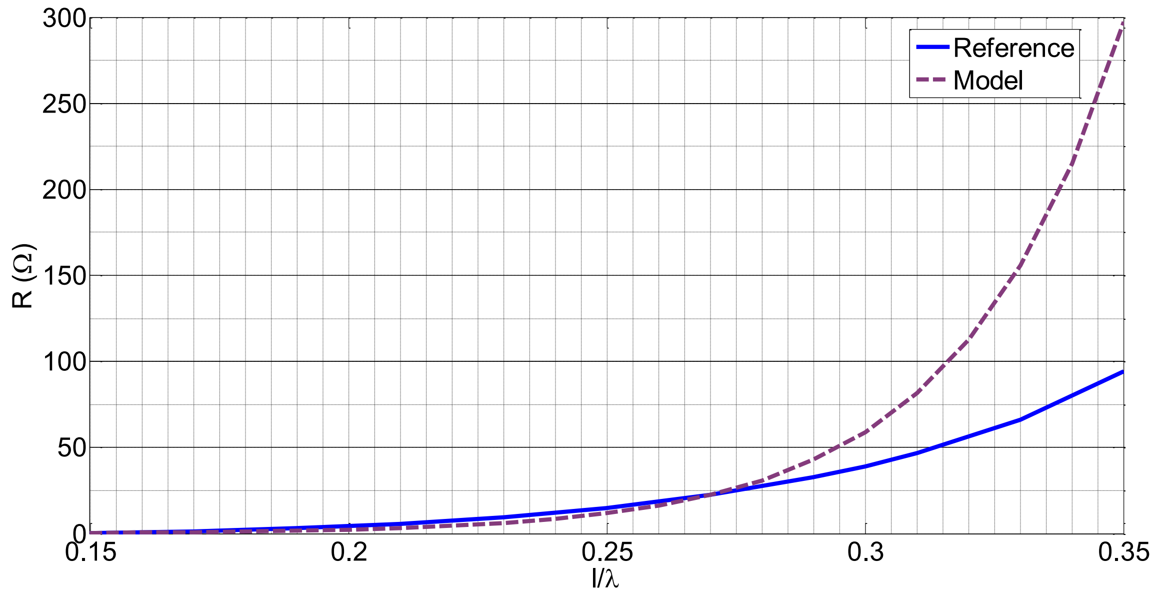

Figure 34: Resistance vs. Electrical length (single leg) of a Meander Dipole Antenna. The “Reference” curve is derived from the simulation of the prototype meander antenna in EMCoS. The “Model” curve represents the radiation resistance of the equivalent circuit derived from the graphical procedure described in *Appendix A*.

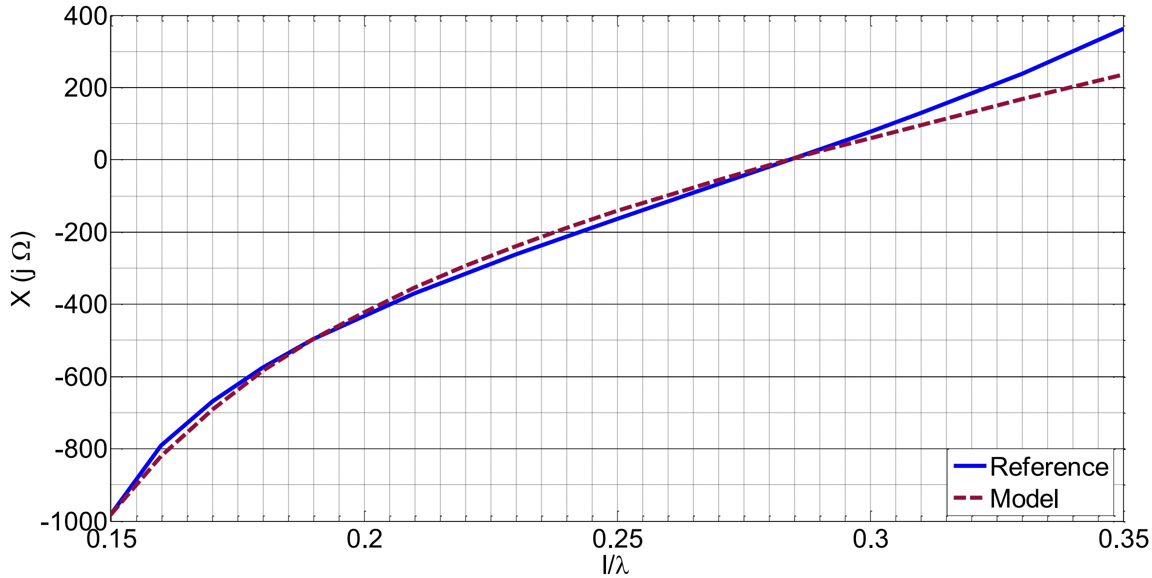

Figure 35: Reactance vs. Electrical length (single leg) of a Meander Dipole Antenna. The "Reference" curve is derived from the simulation of the prototype meander antenna in EMCoS. The "Model" curve represents the reactance of the equivalent circuit derived from the graphical procedure described in *Appendix A*.

In Fig. A.3, the real component of (A.8) which represents the radiation resistance of the meander dipole antenna studied was superimposed on the resistance-electrical length curve obtained by simulation through the EMCoS software. For electrical lengths less than 0.28λ, there was a good agreement between both curves. However, for lengths greater than 0.28λ, there was a divergence of both curves. Since, the antenna designed for the DDA application will be much smaller than wavelength, the $l/\lambda \geq 0.28$ is of no interest to me. Similarly, in Fig. A.4, the imaginary component of (A.13) which represents the total reactance of the meander dipole antenna studied was superimposed on the reactance-electrical length curve obtained by simulation through the EMCoS software. In the region of interest $l/\lambda < 0.28$, there was also a good agreement between the curves.

To demonstrate the effect of meandering on the model of the meander dipole antenna model, suppose the resonant frequency of the prototype antenna studied (see Fig. 4) is known to be 160 MHz. The total length of all the vertical and horizontal segments of a single leg is 55.71 cm. A straight-line dipole will resonate at $l = 0.297\ \lambda_0$. That is, reactance, X is expected to be zero at $l/\lambda = 0.297$. However, for the prototype meander dipole antenna of the same total length as a straight dipole antenna, the point of zero reactance in Figure A.4 is $l/\lambda = 0.284$. The difference in l/λ is due to the difference in the total capacitance of both antenna configurations caused by the mutual coupling of the horizontal segments in a meander antenna.

Appendix B

Calculations of Antenna Radiation Efficiencies

This section contains calculations of the relative efficiencies of the Antenna with Balun (simply referred to as AWB) previously used to evaluate the performance of the Directly-Driven Antenna architecture.

From [50], recall that the radiation efficiency, η_r is defined as

$$\eta_r = \frac{R_r}{R_r + R_l} \tag{5}$$

Where R_r is the radiation resistance and R_l is the loss resistance of the radiating element. The following are the equations used to compute the radiation efficiencies of both antennas. The constants used in the following equations and their definitions can be found in Table B-1 below.

Table B-1: Table of constants.

Antenna	AWB	MDA
Material	Brass	Copper
Conductivity, σ	1.5×10^{7} S/m	5.8×10^{7} S/m
Frequency, f	1.5 MHz	1.5 MHz
Permeability, μo	$4\pi \times 10^{-7}$ H/m	$4\pi \times 10^{-7}$ H/m

Total electrical length, *l*	λ/2200 (9.1 cm)	λ/180 (111.42 cm)
Radius of radiating segments, *a*	1.6 mm	0.525 mm

$$R_r = 80\pi^2\left(\frac{l}{\lambda}\right)^2 \quad \text{(B.1)}$$

$$R_r = 80\pi^2\left(\frac{1}{2200}\right)^2 = 0.163\ m\Omega \quad \text{(AWB)}$$

$$R_r = 80\pi^2\left(\frac{1}{180}\right)^2 = 24.4\ m\Omega \quad \text{(MDA)}$$

$$R_S = \sqrt{\frac{\pi f \mu_O}{\sigma}} \quad \text{(B.2)}$$

$$R_S = \sqrt{\frac{\pi\times1.5\times10^6\times4\pi\times10^{-7}}{1.5\times10^7}} = 0.628\ m\Omega \quad \text{(AWB)}$$

$$R_S = \sqrt{\frac{\pi\times1.5\times10^6\times4\pi\times10^{-7}}{5.8\times10^7}} = 0.32\ m\Omega \quad \text{(MDA)}$$

$$R_l = R_S\left(\frac{l}{2\pi a}\right) \quad \text{(B.3)}$$

$$R_l = 6.28\times10^{-4}\times\left(\frac{0.091}{2\pi\times0.0016}\right) = 5.69\ m\Omega$$
(AWB)

$$R_l = 3.2\times10^{-3}\times\left(\frac{1.1142}{2\pi\times5.25\times10^{-4}}\right) = 0.180\ \Omega$$
(MDA)

Therefore

$$\eta_r = \frac{0.000163}{0.00569+0.000163} = 2.8\% \qquad \text{(AWB)}$$

$$\eta_r = \frac{0.024369}{0.024369+0.108087} = 18.4\% \qquad \text{(MDA)}$$

References

Cited References

[1] R. G. Brown, R. A. Sharpe, W. L. Hughes and R. E. Post, “Lines, Waves, and Antennas,” New York: Wiley, 1973, pp. 339-346.

[2] H. A. Wheeler, "Fundamental Limitations of Small Antennas," *Proceedings of the IRE*, vol.35, no.12, pp. 1479- 1484, Dec. 1947

[3] G. Marrocco, "The art of UHF RFID antenna design: impedance-matching and size-reduction techniques," *IEEE Antennas and Propagation Magazine*, vol.50, no.1, pp.66-79, Feb. 2008.

[4] G.-Y. Lee, Y. Kim, J. Lim, S. Nam, "Size reduction of microstrip-fed slot antenna by inductive and capacitive loading, "*IEEE Antennas and Propagation Society International Symposium, 2003*, vol.1, no., pp. 312- 315 vol.1, 22-27 June 2003.

[5] B. A. Kramer, C.-C. Chen, J. L. Volakis, "Size Reduction of a Low-Profile Spiral Antenna Using Inductive and Dielectric Loading, "*IEEE Antennas and Wireless Propagation Letters*, vol.7, no., pp.22-25, 2008.

[6] J. T. Merenda, “Synthesizer Radiating Systems and Methods,” U.S. Patent 5 402 133, March 28, 1995.

[7] *Class D Audio Amplifiers Save Battery Life*, Maxim Integrated Products, Sunnyvale, CA, AN1760, 2002.

[8] S. El-Hamamsy, “Design of High-Efficiency RF Class-D Power Amplifier,” *IEEE Trans. Power Electron.*, vol. 9,pp. 297–308, May 1994.

[9] F. T. Ulaby, *Electromagnetics for Engineers.* New Jersey: Prentice Hall, 2005, p. 399.

[10] O. O. Olaode, W. D Palmer, and W. T. Joines, “Improvements of a Directly-Driven Antenna-Based AM Transmitter over the AM Frequency Band,” *Proceedings of the 2010 Antenna Applications Symposium*, vol. 34, pp. 372-388, Sept. 2010.

[11] W. L. Stutzman and G. A. Thiele, *Antenna Theory and Design*, 2nd ed. New York: Wiley, 1998.

[12] H. Nakano, J. Yamauchi, H. Mimaki, "Backfire radiation from a monofilar helix with a small ground plane," *IEEE Transactions on Antennas and Propagation*, vol. 36, no. 10, pp. 1359-1364, Oct 1988.

[13] R. Vaughan, J. Andersen, "Polarization properties of the axial mode helix antenna," *IEEE Transactions on Antennas and Propagation,* vol. 33, no. 1, pp. 10- 20, Jan. 1985.

[14] W. T. Patton, "The backfire bifilar helical antenna", University of Illinois Antenna Lab. Technical Report 61, 1962.

[15] H. Nakano, Y. Samada, J. Yamauchi, "Axial mode helical antennas," *IEEE Transactions on Antennas and Propagation*, vol. 34, no. 9, pp. 1143- 1148, Sep. 1986.

[16] A. Adams, R. Greenough, R. Wallenberg, A. Mendelovicz, C. Lumjiak, "The quadrifilar helix antenna," *IEEE Transactions on Antennas and Propagation*, vol. 22, no. 2, pp. 173- 178, Mar. 1974.

[17] R. Sainati, J. Groppelli, R. Olesen, A. Stanland, "A band-switched resonant quadrifilar helix," *IEEE Transactions on Antennas and Propagation*, vol.30, no.5, pp. 1010- 1013, Sep. 1982.

[18] S. H. Zainud-Deen, N.A.-D.M. Salem, S. M. M. Ibrahem, H. A. Motaafy, "Investigation of an octafilar helix antenna," *Proceedings of the Nineteenth National Radio Science Conference, 2002*, pp. 72-80, 2002.

[19] J. M. Tranquilla, S. R. Best, "A study of the quadrifilar helix antenna for Global Positioning System (GPS) applications," *IEEE Transactions on Antennas and Propagation*, vol. 38, no.10, pp. 1545-1550, Oct. 1990.

[20] C.-W. Lan, T.-H. Chang, J.-F. Kiang, "Helical antenna for GPS applications," *IEEE Antennas and Propagation Society International Symposium, 2004*, vol.3, no., pp. 3329- 3332, June 2004.

[21] A. Mirkamali, L. Akhoondzadeh, K. Keyghobad, M. Soleimani, "A novel quadrifilar helix antenna for use in LEO satellite communications," *4th International Conference on Antenna Theory and Techniques*, vol. 2, pp. 509- 511, Sept. 2003.

[22] P. Y. Lau, H. Wong, E. K. N. Yung, "Accordion shape monofilar axial mode helix for RFID reader," *Electronics Letters*, vol. 42, no. 11, pp. 607- 608, May 2006.

[23] D. K. C. Chew, S. R. Saunders, "Meander line technique for size reduction of quadrifilar helix antenna," *IEEE Antennas and Wireless Propagation Letters,* vol. 1, no. 1, pp. 109-111, 2002.

[24] B. Bhandari, S. Gao, T. Brown, "Meandered Variable Pitch angle Printed Quadrifilar Helix Antenna," *Loughborough Antennas & Propagation Conference, 2009*, pp.325-328, Nov. 2009.

[25] Y.-S Wang, S.-J Chung , "A Miniature Quadrifilar Helix Antenna for Global Positioning Satellite Reception," *IEEE Transactions on Antennas and Propagation*, vol. 57, no. 12, pp. 3746-3751, Dec. 2009.

[26] W. G. Hong, W. H. Jung, Y. Yamada, N. Michishita, "High performance normal mode helical antennas for RFID tags," *2007 IEEE Antennas and Propagation Society International Symposium*, pp.6023-6026, June 2007.

[27] D. B. Miron, *Small Antenna Design.* Burlington, MA: Newnes, 2006.

[28] J. D. Kraus, *Antennas.* New York: McGraw-Hill, 1950, p. 713.

[29] K. Asakura, S. Kanba, T. Tsuru, and H. Mandai, "Meander Line Antenna," U.S. Patent 5,892,490, April 6, 1999.

[30] T. Williams, M. Rahman, and M. A. Stuchly, "Dual-band meander antenna for wireless telephones," *Microwave and Optical Technology Letters*, vol. 24, no. 2, pp. 81- 85, Jan. 2000.

[31] K. V. S. Rao, P. V. Nikitin, and S. F. Lam, "Antenna design for UHF RFID tags: a review and a practical application," *IEEE Transactions on Antennas and Propagation*, vol.53, no.12, pp. 3870- 3876, Dec. 2005.

[32] M. Hamid, and R. Hamid, "Equivalent circuit of dipole antenna of arbitrary length," *IEEE Transactions on Antennas and Propagation*, vol. 45, no. 11, pp. 1695-1696, Nov. 1997.

[33] G. W. Streable and L. W. Pearson, "A numerical study on realizable broad-band and equivalent admittances for dipole and loop antennas," *IEEE Transactions on Antennas and Propagation,* vol. AP-29, no. 5, pp. 707-117, September 1981.

[34] B. Long, P. Werner, D. Werner, "A simple broadband dipole equivalent circuit model," *IEEE Antennas and Propagation Society International Symposium, 2000*, vol. 2, pp. 1046-1049, 2000.

[35] T. Endo, Y. Sunahara, S. Satoh, and T. Katagi, "Resonant frequency and radiation efficiency of meander line antennas," *Electron. Commun. Jpn.*, Part II 83, 2000.

[36] D. Puente, D. Valderas, J. Garcia, J. Melendez, J. Gomez, and J. I. Sancho, "Resonant frequency calculation of meander dipole antennas by TLM," *Microw. Opt. Techn. Lett.*, vol. 50, no. 6, Jun. 2008.

[37] S. R. Best, J.D. Morrow, "Limitations of inductive circuit model representations of meander line antennas," *IEEE Antennas and Propagation Society International Symposium, 2003,* vol.1, pp. 852- 855, 22-27 June 2003.

[38] T. J. Warnagiris, and T. J. Minardo, "Performance of a Meandered Line as an Electrically Small Transmitting Antenna," *IEEE Transactions on Antennas and Propagation,* vol. 46, no. 12, Dec. 1998.

[39] T. G. Tang, Q. M. Tieng, M. W. Gunn, "Equivalent circuit of a dipole antenna using frequency-independent lumped elements," *IEEE Transactions on Antennas and Propagation,* vol. 41, no. 1, pp.100-103, Jan 1993.

[40] EMCoS Antenna VirtualLab, EMCoS Ltd., Tblisi, Georgia. http://www.emcos.com.

[41] H. Nakano, H. Tagami, A. Yoshizawa, J. Yamauchi, "Shortening ratios of modified dipole antennas," *IEEE Transactions on Antennas and Propagation,* vol. 32, no. 4, pp. 385- 386, Apr 1984.

[42] R. King, C. W. Harrison, Jr, "The Distribution of Current along a Symmetrical Center-Driven Antenna," *Proceedings of the IRE*, vol. 31, no. 10, pp. 548- 567, Oct. 1943.

[43] J. Rashed, J, C.-T Tai, "A new class of resonant antennas," *IEEE Transactions on Antennas and Propagation*, vol.39, no.9, pp.1428-1430, Sep 1991.

[44] C. A. Balanis, *Antenna Theory: Analysis and Design*. Hoboken, NJ: John Wiley & Sons, Inc., 2005.

[45] FEKO Suite 6.2, EM Software & Systems-S.A. (Pty) Ltd., Cape Town, South Africa. http://www.feko.info.

[46] M. Ali, S. S. Stuchly, "A meander-line bow-tie antenna," Antennas and Propagation Society International Symposium, 1996. AP-S. Digest , vol.3, pp.1566-1569, Jul. 1996.

[47] J.-F Li, B.-H. Sun, H.-J. Zhou, and Q.-Z. Liu, "Miniaturized circularly-polarized antenna using tapered meander-line structure," *Progress in Electromagnetics Research*, vol. 78, 321–328, 2008.

[48] Jampro Antennas, Inc., “Return loss conversion table”, *Technical Documents*, http://www.jampro.com/uploads/tech_docs_pdf/VSWRChart.pdf.

[49] Conversation with Prof. Joines.

[50] D. K. Cheng, *Field and Wave Electromagnetics*. Reading, MA: Addison-Wesley, 1989, p. 613.

[52] NI Multisim 11, National Instruments, Austin, TX. www.ni.com/multisim.

Non-Cited References

The following are the references that were not cited in the body of the dissertation but enhanced my understanding of the relevant concepts needed to perform the work therein.

[1] G. Breed, “Basic Principles of Electrically Small Antennas,” High Frequency Electronics, February 2007. http://www.highfrequencyelectronics.com/Archives/Feb07/HFE0207_tutorial.pdf

[2] R. Schmitt, “Understanding electromagnetic fields and antenna radiation takes (almost) no math,” *EDN Magazine*, January 1970. http://www.edn.com/file/21352-82250.pdf.

[3] J. P. Donohoe, “Loop Antennas,” *Lecture Notes, Mississippi State University*. http://www.ece.msstate.edu/~donohoe/ece4990notes5.pdf.

[4] K. Rambabu, M. Ramesh, A. T. Kalghatgi, "Broadband equivalent circuit of a dipole antenna," *IEE Proceedings - Microwaves, Antennas and Propagation*, vol.146, no.6, pp.391-393, December 1999.

[5] A. A. Lestari, A. G. Yarovoy, L. P. Ligthart, "An Efficient Ultra-Wideband Bow-Tie Antenna," *31st European Microwave Conference,2001*, vol., no., pp.1-4, 24-26 September 2001.

[6] S. D Keller. *Design and Development of Directly-Modulated Antennas using High-Speed Switching Devices*. PhD thesis, Duke University, 2008.

[7] W. D. Palmer, “Direct Antenna Modulation: Analysis, Design, and Experiment” *Army Research Office Progress Report*, 2011.

[8] “High-Efficiency Class D Audio Amplifiers Extend Battery Life in Portable Applications,” *Technical Report*, 2010. http://pdfserv.maximintegrated.com/en/an/AN1760.pdf.

[9] W. T. Joines, Microwave Electronic Circuits, *Class Notes*, 2007.

[10] W.T. Joines, Elements of Electromagnetic Communications, *Class Notes*, 2009.

[11] M. J. Wilson, The ARRL Handbook for Radio Communications (86th edition), ARRL – The National Association for Amateur Radio, 2009.

Biography

Olusola O. Olaode was born in Ibadan, Nigeria. He received the B.S. degree in electrical engineering from Rochester Institute of Technology, Rochester, NY, in 2006 and the M.S. degree in electrical and computer engineering from Duke University, Durham, NC, in 2008. He is currently a doctoral candidate in electrical and computer engineering at Duke University. He has held several intern positions with the Brookhaven National Laboratory of the US Department of Energy, Intel Corporation and Northrup Grumman Electronic Systems. His research interests include investigation of electrically-small antennas for defense applications. Mr. Olaode is a member of the Phi Theta Kappa honors society, Institute of Electrical and Electronics Engineers and the National Society of Black Engineers. He is a National GEM Consortium Doctoral Fellow.

Publications and Presentations

- O. O. Olaode, W. D. Palmer, and W. T. Joines, "Evaluating the Efficiency of the Digitally-Driven Antenna Architecture," *IEEE International Symposium on Antennas and Propagation and Union of Radio Science International Meeting*, Charleston, SC – June 2009.
- O. O. Olaode, "Analysis of the Efficiency Improvements of a Directly-Driven Antenna-Based AM Transmitter," *Antenna Applications Symposium*, Monticello, IL, Sept. 2009, poster presentation.
- O. O. Olaode, W. D. Palmer, and W. T. Joines, "Analysis of the Efficiency Improvements of a Directly-Driven Antenna-Based AM Transmitter," *Proceedings of the 2009 Antenna Applications Symposium*, vol. 33, pp. 418-429, Sept. 2009.
- O. O. Olaode, W. D. Palmer, and W. T. Joines, "Improvements of a Directly-Driven Antenna-Based AM Transmitter over the AM Frequency Band," *Proceedings of the 2010 Antenna Applications Symposium*, vol. 34, pp. 372-388, Sept. 2010.

- O. O. Olaode, “Efficiency Improvements of a Directly-Driven Antenna-Based AM Transmitter over the AM Frequency Band,” *Proceedings of the 2010 Antenna Applications Symposium*, Monticello, IL, Sept. 2010, poster presentation.
- O. O. Olaode, W. D. Palmer, and W. T. Joines, “Efficiency Improvements of a Directly-Driven Antenna-Based AM Transmitter over the AM Frequency Band,” *IEEE Antennas and Propagation Society Meeting*, Spokane, WA, July 2011.
- O. O. Olaode, W. D. Palmer, and W. T. Joines, “Effects of Meandering on Dipole Antenna Resonant Frequency,” *IEEE Antennas and Wireless Propagation Letters*, accepted for publication, January 2012.
- O. O. Olaode, W. D. Palmer, and W. T. Joines, “Characterization of Meander Dipole Antennas with Geometry-based, Frequency-independent Lumped Element Model,” *IEEE Antennas and Wireless Propagation Letters*, March 2012.
- W. D. Palmer, O. O. Olaode, R. J. Spiegel, and W. T. Joines, “Directly-Driven Antennas from a Circuit Analysis Viewpoint,” *Proceedings of the 2011 Antenna Applications Symposium*, September 2011.